Master's Thesis

SMD Simulation of Talin and Integrin Interaction – Role of membrane proximal and distal integrin segments in talin binding

Lassi Palmujoki

University of Jyväskylä

Department of Biological and Environmental Science

Cell and Molecular Biology

24 November 2022

UNIVERSITY OF JYVÄSKYLÄ, Faculty of Mathematics and Science
Department of Biological and Environmental Science

Degree programme:	Master's Degree Programme in Cell and Molecular Biology
Palmujoki, Lassi	SMD Simulation of Talin and Integrin Interaction – Role of membrane proximal and distal integrin segments in talin binding
MSci Thesis	49 pages, 1 appendix (6 pages)
Supervisors:	prof. Vesa Hytönen, prof. Jari Ylänne, PhD Vasyl Mykuliak
Reviewers:	University lecturer Ulla Pentikäinen, Academy Research Fellow Heikki Takala

November 2022

Keywords: computational biology, mechanobiology

The area of molecular biology dealing with physical forces is a rapidly advancing field, thanks to technology that is getting faster and improvements in theoretical fronts like computational simulations of molecular systems - particularly steered molecular dynamics (SMD) simulations and related methods. SMD allows similar and extended ways to study molecular (un)binding and (un)folding processes like atomic force microscopy (AFM) and magnetic tweezers. However, due to limitations in computer hardware (for the time being) the forces are several orders of magnitude larger than those observed with experimental methods and, unfortunately, quantitative results are either very challenging or impossible to acquire. Being qualitative in nature, however, information on the precise atom-level evolution of molecular interactions can be obtained that is also meaningful outside the context of a single experiment. This study deals with the evolution of interactions, as determined by SMD, between proteins talin-1 and integrin beta3, particularly the interaction between talin-1 FERM-folded head domain and the cytoplasmic segment of integrin beta3. The study aimed to answer two research questions: 1) Is the pulling force acquired from SMD simulations a single- or multi-step process? In other words, how many energy barriers does the pulling force profile contain? 2) When observing the unbinding process for talin and integrin in reverse (i.e., binding), does this binding process correlate to the previously proposed binding model? This is the second study to utilize the similar computational method (SMD) for the analysis of that particular interaction. However and to the best of our knowledge, the talin-1 FERM structure used in this study better resembles a biologically existing talin structure than those used in previous studies. Also, in contrast to previous studies, the whole cytoplasmic segment of integrin beta3 is utilized in this study, which results from combining the membrane proximal and membrane distal parts of integrin beta3 from different crystallographic structures. The SMD simulations of the unbinding and unfolding of talin1-integrin beta3 interaction suggest a two-step process. The first energy barrier, observed as a peak in the pulling force profile, corresponds to the unbinding of the membrane proximal helix, which becomes unstable and unfolds under load during unbinding. The unbinding of the NPLY motif in the membrane distal part is, likewise, associated with the second energy barrier. When observing the trajectory in reverse the results support the previously proposed hypothesis that the talin-integrin interaction is based on the initial binding of the NPLY motif followed by the binding of the membrane proximal segment of integrin to talin.

JYVÄSKYLÄN YLIOPISTO, Matemaattis-luonnontieteellinen tiedekunta
Bio- ja ympäristötieteiden laitos

Tutkinto-ohjelma:	Solu- ja molekyylibiologian maisteriohjelma
Palmujoki, Lassi	SMD-simulaatio taliinin ja integriinin vuorovaikutuksesta - Integriinin kalvoläheisen ja kalvokaukaisen segmentin rooli taliiniin sitoutumisessa
Pro gradu tutkielma	49 sivua, 1 liite (6 sivua)
Työn ohjaajat:	prof. Vesa Hytönen, prof. Jari Ylänne, PhD Vasyl Mykuliak
Tarkastajat:	Yliopistolehtori Ulla Pentikäinen, dosentti Heikki Takala
Marraskuu 2022	

Hakusanat: laskennallinen biologia, mekanobiologia

Fyysisiä voimia käsittelevä molekyylibiologian alue on nopeasti kehittymässä, johtuen sekä tietokoneiden laskentakapasiteetin kasvusta että kehityksistä teoreettisilla rintamilla kuten molekyylijärjestelmien laskennallisessa simulaatiossa – eritoten ohjatun molekyylidynamiikan (steered molecular dynamics, SMD) ja sen kaltaisten menetelmien osalta. SMD mahdollistaa samankaltaisen, mutta osaltaan yksityiskohtaisemman tavan tarkastella molekyylien sitoutumista ja irtoamista verrattuna kokeellisiin menetelmiin, kuten atomivoimamikroskooppi ja magneettiset pinsetit (magnetic tweezers). Tietokoneiden laskentakapasiteetin rajat tulevat kuitenkin (toistaiseksi) vastaan siinä määrin, että voimien on oltava useita suuruusluokkia suurempia kuin kokeellisissa menetelmissä. Osaltaan tästä johtuu, että määrällisiä tuloksia on joko erittäin vaikea, ellei mahdoton saada. Vaikkakin tulokset ovat laadullisia, tietoa täsmällisestä atomitason vuorovaikutusten kehityksestä on mahdollista saada, ja tämä tieto on mielekästä myös kokeen viitekehyksen ulkopuolella. Tässä tutkimuksessa käsitellään SMD:llä määritettyä vuorovaikutusten kehitystä kahden proteiinin, taliini-1:n ja integriini beta3:n, välillä; tarkemmin ottaen taliini-1:n FERM-laskoksisen päädomeenin ja integriini beta3:n sytoplasmisen häntädomeenin välillä. Tutkielma pyrkii vastaamaan kahteen tutkimusongelmaan: 1) Onko SMD:llä määritetty vetovoima (pulling force) yksi- vai monivaiheinen prosessi? Eli kuinka monta energiakynnystä on vetovoimakuvaajassa? 2) Tarkasteltaessa taliinin ja integriinin irtoamisprosessia käänteisessä suunnassa (eli niiden sitoutumisprosessia), korreloiko tämä sitoutumisprosessi aiemmin esitetyn sitoutumisprosessin kanssa? Tämä on toinen tutkimus, joka hyödyntää samankaltaista laskennallista menetelmää (SMD) kyseisen proteiinivuorovaikuksen analyysiin. Kuitenkin parhaan tietomme mukaan taliini-1:n FERM-rakenne vastaa nyt paremmin biologisesti ilmenevää rakennetta kuin aikaisemmissa tutkimuksissa. Sen lisäksi, toisin kuin aikaisemmissa vastaavissa tutkimuksissa, tässä tutkimuksessa hyödynnetään integriini beta3:n koko sytoplasmista häntädomeenia yhdistämällä kalvoläheisen (membrane proximal) ja kalvokaukaisen (membrane distal) osan eri kristallografiarakenteista. Taliini-1-integriini beta3-vuorovaikutuksen SMD-simulaatio vaikuttaa olevan kaksiaskelinen prosessi. Ensimmäinen energiakynnys vastaa kalvoläheisen osan irtoamista taliinista, kun taas integriinin NPLY-osan irtoaminen osuu toisen energiakynnyksen kohdalle. Liikeradan tarkastelu käänteisessä suunnassa tukee aiemmin ehdotettua hypoteesia, että taliini-integriini-vuorovaikutus perustuu alustavaan NPLY-osan sitoutumiseen, jota seuraa kalvoläheisen osan sitoutuminen taliiniin.

TABLE OF CONTENTS

1 INTRODUCTION

1.1 Mechanobiology

Cells are immersed in varying 3D environments in multicellular organisms (Bowers et al. 2010). Osteoclasts reside in hard, unyielding bone tissue (Alford et al. 2015), whereas neurons of the brain reside in far softer, supple brain tissue (Barnes et al. 2017), and fibroblasts reside in connective tissues of varying stiffness (Humphrey et al. 2014). Bone remodeling is dependent on gravity and impact; without those cues, bone starts to lose mass (Hill, 1998) and physical strain is required to build muscles (Tidball, 2005). Likewise, physical pressure in the inner ear becomes translated into chemical and nerve signals (Maoiléidigh and Ricci, 2019), while stem cells in developing individuals differentiate into particular cells based not only on chemical signals but also the tissue's mechanical stiffness (Lee et al. 2011).

All of these examples are in the domain of mechanobiology, a multidisciplinary field involving physics and biology that focuses on associating physical forces with biological phenomena (Wang and Thampatty, 2006).

The effect of the mechanical force can be studied at the level of a single molecule, individual cells, and whole tissue. There are several experimental methods of probing single-molecule forces, such as optical tweezers (Tan et al. 2012) and atomic force microscopy (Krieg et al. 2019). One method to analyze the mechanical properties of the cell is to engineer the cell microenvironment in vitro – for example, cell lines developing from stem cells may have different fates based on the stiffness of the cell microenvironment (Lund et al. 2009). However, owing to the difficulty of probing forces in vivo and of replicating the complex natural 3D tissue environments in vitro, much of the mechanobiological processes remain poorly understood. Molecular dynamics simulation, the approach to be applied in the proposed study, offers one way of overcoming the problem at the molecular level (Mak et al. 2015). The key proteins involved in my study are integrin and talin, which are only two proteins of the about 150 known to be involved in integrin-mediated adhesions, but naturally this complex is in a key position in adhesion mechanosignalling since cells devoid

of talin are non-adherent and adhesion signaling does not take place (Theodosiou et al. 2016).

1.2 Integrin

Integrin is involved in cellular contact with the extracellular matrix (ECM) and in the inside–out and outside–in signaling of information about intracellular and extracellular conditions (Lau et al. 2009; Hytönen & Wehrle-Haller, 2016). In particular, integrin, a heterodimeric single-pass transmembrane protein, binds ECM fibers and numerous intracellular adaptor proteins that link it to actin cytoskeleton (Morse et al. 2014). There exist 24 different integrin heterodimers in mammals each with its own intracellular and extracellular binding partners. Less complex species have progressively fewer integrins (Takada et al. 2007). Integrin is an important factor in development and normal physiology as well as in conditions conducive to disease (van der Flier & Sonnenberg, 2001). Except for cancer cells, cells generally cannot proliferate without integrin signals (a phenomenon called "anchorage dependence"), and the loss of integrin signaling causes cell apoptosis (Schwartz, 1997).

The 24 mammalian heterodimeric integrins consist of different combinations of 18 α-integrins and 8 β-integrins. Both α- and β-chains consist of a large extracellular domain (more than 1600 amino acids), one short membrane crossing segment, and a generally short intracellular domain (20-70 amino acids), with the exception of β4 integrin, which has an intracellular domain of 1000 amino acids (Takada et al. 2007). The β integrin cytoplasmic tails are generally conserved, whereas in α tails only a specific GFFKR motif is conserved. The αβ-integrins can be divided into several categories based on, e.g., the extracellular binding partner or ligand (Humphries et al. 2006; Bachmann et al. 2019). First, perhaps the most studied ligand is Arg-Gly-Asp (or RGD) tripeptide-containing ligand, which binds to 8 of the 24 integrins (Ruoslahti & Pierschbacher 1987; Nieberler et al. 2017; Ludwig et al. 2021). Both α and β chains take part in binding the RGD. RGD tripeptide is expressed, e.g., in ECM proteins fibronectin, vitronectin, and laminin. The β3 integrin central to the current study also binds RGD ligands (Horton, 1997). Second, another short integrin ligand peptide is Lys-Asp-Val (or LDV) (Tselepis et al. 1997), which actually has a consensus sequence L/I-D/E-V/S/T-P/S (Humphries et al. 2006). In different integrins it is bound either by both α and β chains (likewise in RGD) or the A-domain of integrin α. Third, another subfamily of integrins binds laminin and collagen (Calderwood et al. 1997). Those integrins also have

embedded A-domain in the integrin α and pair with β1 integrin. Fourth, yet another subfamily also binds laminin, but those do not have the A-domain and bind to a different region of laminin (Humphries et al. 2006).

1.3 Talin

Talin is an adaptor protein that binds integrin's cytoplasmic tail and actin cytoskeleton either directly or via vinculin (Sun et al. 2019). Talin contains numerous binding sites for other proteins, some of which emerge when mechanical tension stretches the protein (Del Rio et al. 2009). Talin is also often required in the activation of integrin into high-affinity conformation (Calderwood et al. 1999) and induces integrin clustering (Cluzel et al. 2005). By initiating intracellular signaling cascades, talin thus links mechanical signals and chemical signals (Goult et al. 2018). Together, integrin and talin are two major players in focal adhesions (Klapholz and Brown, 2017)—that is, large complexes of several dozen different proteins involved in cell–ECM adhesion and cellular migration.

Two talin isoforms exist: talin-1 and talin-2. Even though the genes of the proteins supposedly diverged before the divergence of jawed and jawless vertebrates, the two proteins are 76% identical, contain approximately 2540 amino acids, and have similar domain structures, each with 18 domains (Gough and Goult, 2018). However, the gene for talin-2 contains far larger introns than talin-1 and numerous splice variants that are currently little studied. Mice with the talin-1 knockout do not live past the embryonic state, whereas mice with the talin-2 knockout develop normally and are fertile, though their offspring do not survive to adulthood, just as their parents (Debrand et al. 2012). The expression of the two talins is also markedly different: talin-1 is ubiquitously expressed in nearly all cells of the body, whereas talin-2 is found primarily in the brain, heart muscle, and kidneys (Gough and Goult, 2018).

Talins are 270-kDa proteins consisting of a head domain that is ~50-kDa FERM fold (4.1 protein, ezrin, radixin, and moesin fold), with F0, F1, F2, and F3 subdomains, along with a linker sequence and a ~220-kDa rod domain consisting of 13 helical bundles of four to five α-helices. Despite earlier evidence suggesting that the FERM fold was atypically linear (Elliott et al. 2010), a more recent study proposes that F1–F2–F3 fold into the typical cloverleaf form with the addition of F0 (Zhang et al. 2020). The F3 domain interacts with

integrin β's cytoplasmic tail, including integrin β's proximal α-helix and NPxY motif (Kääpä et al. 1999; Saltel et al. 2009). Earlier it was thought that the talin head domain alone is enough to activate integrin (Calderwood et al. 1999), but more recent studies support the proposition that kindlin and mechanical forces are also highly important in the process. Meanwhile, talin is anchored in a correct position in the cell membrane by F2–F3 subdomains that interact with PIP2 phospholipids in the cell membrane, and F0 that interacts with membrane-tethered Rap1 GTPase (although a more recent finding questions that observation; Lagarrigue et al. 2018). It is the effect of these PIP2 lipids that also releases talin from its autoinhibitory binding (Wang, 2012). Talin's rod domain has a binding site for integrin, two binding sites for actin, and 11 binding sites for vinculin, the last of which are revealed by mechanically stretching talin and by unfolding the helical bundles (Del Rio et al. 2009; Haining et al. 2016; Yao et al. 2016). Several other proteins bind to talin in its relaxed state, including paxillin, DLC1, RIAM, and KANK. The different binding partners for stretched and relaxed talin mediate different states of the adhesion site's maturation (Atherton et al. 2020).

1.4 Integrin and talin activity regulation

The proper function of cell adherence is dependent on delicate control of integrin and talin activity. The chain of events that lead to active integrin and talin, both of which exist natively in auto-inhibited conformation (Klapholz & Brown, 2017), remains unclear. Multiple pathways of activation seem to exist in different tissues and for different integrins. Mutational studies have revealed that some of the integrins cause developmental defects in Drosophila embryos if they have mutated to become constitutively active (Martin-Bermudo et al. 1998). Moreover, it was shown (Bachmann et al. 2020) that mechanical force is an important factor directing the selectivity of integrin. Thus, in some cases - if not all - controlling integrin's activity is paramount. Knockout studies of embryos lacking talin have revealed defects similar to those caused by integrin's absence, even though integrin adheres to the ECM. Other molecules that can activate those integrins inside–out or are activated by binding with ECM seem to exist as well (Campbell & Humphries, 2011). Kindlin was reported to be as potent an integrin activator as talin, and more important than talin in subsequent intracellular signaling leading to focal adhesion formation (Theodosiou et al. 2016).

Figure 1 depicts the three conformational states of integrin: bent closed (inactive), extended closed (inactive), and extended open (highly active) (Chen et al. 2010; Sun et al. 2019). The term "active", in the case of integrin signaling, refers to the binding affinity to extracellular ligands. One possible initial activator is talin, capable of "inside-out" integrin activation (Wegener et al. 2007). Autoinhibited talin is assumed to get activated by interaction with PIP2 lipids in the cell membrane, which leads to the unveiling of the FERM F3 domain of talin, which, in turn, binds the integrin β cytoplasmic tail via the NPLY motif. This talin F3-β integrin tail interaction is reported to cause the unbinding of a salt bridge between α and β integrins (αIIb(R995)–β3(D723)), which leads to the separation of the two integrin chains (Hughes et al. 1996). Upon activation, integrin adopts an extended conformation and further activation to the open state is known to happen via the outside-in route, where the integrin head binds the ECM ligand, which causes the integrin legs, transmembrane domains, and cytoplasmic tails to separate, potentially facilitated by the talin F1 loop (Kukkurainen et al. 2020).

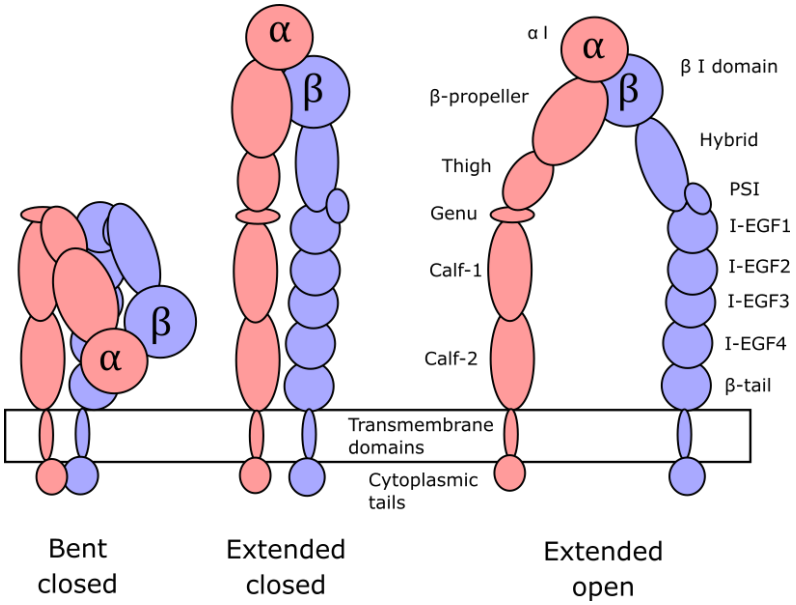

Figure 1. Three conformational states of integrin. Bent closed and extended closed correspond to the inactive state (low affinity to ECM ligands) and extended open to an active state (high affinity to ECM ligands).

1.5 Integrin clustering

As important as activating integrins into a high-affinity state is integrin clustering, which is another means by which cells adhere strongly to the ECM at specific locations. Integrin clustering, which seems to depend on molecular factors such as ECM ligands, Mn2+ and

intracellular factors including talin, can also be induced by directed mutation on integrin (Cluzel et al. 2005). Integrin αvβ3 clustering, for example, depends on extracellular fibronectin or vitronectin and does not cluster in the presence of other cluster-inducing factors if ECM consists of laminin-1. In their research on integrin clustering, Cluzel et al. (2005) also found that among the focal adhesion adaptor proteins — talin, vinculin, paxillin and FAK — as well as anti-phosphotyrosine antibodies, only talin initially associated with the integrin clusters induced by Mn2+ or mutagenesis. The other adaptor proteins, meanwhile, seemed to depend on the subsequently formed talin–actin connection. Other work has also revealed that the auto-inhibition of talin seems to be released by cell membrane-bound lipid PI(4,5)P2, thus activating talins in the cell periphery where integrin adhesions form (Martel et al. 2001).

1.6 Focal adhesions and other adhesive integrin complexes

Integrin and talin are part of multiprotein complexes with possibly more than 150 different proteins (Zaidel-Bar et al. 2007) that link ECM fiber proteins to the intracellular actin cytoskeleton and relay information both inside-out (about the cytoplasmic state to the outside of the cell) and outside-in (about the extracellular state to cytoplasm). The mature form of such a complex is known as focal adhesion (FA) or fibrillar adhesion, and before that it is called focal complex or, in an even earlier state, nascent adhesion (Burridge, 2017). FA contains proteins associated with cell cytoskeleton (e.g., talin, vinculin, paxillin, α-actinin), in phosphorylation (e.g., FAK, Src, ILK), in dephosphorylation (e.g., SHP-2) and proteolysis (e.g., calpain). Together the proteins form an extensive signaling network that regulates the activity of the FA proteins and the turnover rate of the focal adhesions (Ren et al. 2000; Saunders et al. 2006).

The controlled construction and deconstruction of focal adhesions is especially important in cell migration, both in normal and disease conditions (Nagano et al. 2012), which involve the constant construction of FAs in the leading edge and the deconstruction in the trailing edge (Lauffenburger and Horwitz, 1996). The mechanism of this dynamic behavior is not well known, but apparently the role of calpain protease is important in breaking apart the FA (Franco et al. 2004; Chan et al. 2010). An essential factor in the maturation of FA is the mechanical force sensed by the adhesion (Stricker et al. 2013). For example, there might be a different extent of rigidity in the extracellular substrate around the cell and, with the

application of force by the actomyosin contractile cytoskeleton, the adhesions sense a different amount of stress. This difference in sensed stress is the basis for durotaxis, in which the cells form FAs in the sites of higher rigidity and thus migrate toward that higher rigidity substrate (Rens and Merks, 2020). A recent study linked talin expression level and durotaxis (Isomursu et al. 2022).

In addition to the family of FA type of integrin adhesions, there exists a family of podosome type adhesions (PTA) (Block et al. 2008). This family consists of podosomes and invadopodia, although it is currently a matter of debate whether the two are actually one single structure in different kinds of cellular conditions. Nevertheless, there is a convention to call the structure "podosome" if it appears in non-cancer cells and "invadopodium" if it appears in cancer cells (Murphy and Courtneidge, 2011). PTAs contain a set of proteins very similar to FAs, e.g., integrin, talin, and paxillin (Block et al. 2008). Both types of adhesion complexes serve to bind intracellular actin cytoskeleton to ECM proteins via integrin (and possibly via other non-identified receptors) in the plasma membrane. A major difference is how the actin filaments are organized in the complex: in FAs actin is in the form of tangential stress fibers that can contract and thus induce force from the cell interior, while actin in PTAs forms a thick, conical complex perpendicular to the plasma membrane. Another difference is that PTAs can break apart ECM proteins (Vincent et al. 2012). Such action is crucial when the organism develops from an embryo onwards, and cells (such as neurons) need to migrate through a tissue microenvironment. ECM disintegration is also important in grown-up organisms, such as in wound healing (Michopoulou et al. 2020). In turn, cancer cells form invadopodia to hazardously migrate through the tissues here and there in the organism (Buccione et al. 2009).

1.7 Integrin-talin interface

Although the two proteins involved are relatively large, the binding interface is rather limited in extent (Anthis et al. 2010). The part of integrin involved in the interface is its short cytoplasmic domain (or tail) of the β subchain. In particular, the parts of the tail that make connections to talin are the NPLY-motif of the membrane distal segment (García-Alvarez et al. 2003) and the membrane proximal helix (Wegener et al. 2007). Talin, in turn, has a so-called PTD- (phosphotyrosine binding) like interface in its F3 subdomain that binds the NPLY-motif (Calderwood et al. 2002). The membrane proximal helix of integrin is also

bound by the F3 subdomain. The original peptide found to bind the PTB domain was Asn-Pro-X-pTyr (or phosphorylated Tyr) and the talin version of the PTB deviates from that by binding nonphosphorylated Tyr. Thereafter, different PTB were found to bind a more varied group of peptides (Forman-Kay and Pawson, 1999).

1.8 Structure of study and computational model

My research involves the study of the interaction between cytoplasmic β3-integrin and FERM-folded head domain of talin-1 by means of steered molecular dynamics (SMD) simulation. The starting structure was the experimentally acquired talin-1-β3-integrin complex (P. Zhang et al. 2020). Unlike prior talin structures, this structure contains a clover-like fold like the rest of the known FERM domain proteins. The complex in the crystal is stabilized by the covalent binding of the integrin to the N-terminal part of the talin, but the non-covalent talin-integrin binding appears to reproduce the predicted talin-integrin interface. A superimposition was performed with a dozen experimentally determined F3 subdomains to test whether the talin F3 domain structure used in the current study resembles those determined earlier (2K00, Wegener et al. 2008; 2MWN, Yang et al. 2017; 2KGX, Goult et al. 2009; 1MIX, García-Alvarez et al. 2003; 2H7E, Wegener et al. 2007; 6U4K, Rangarajan et al. 2020; 6R9T, Dedden et al. 2019; 1MK7, García-Alvarez et al. 2003; 6VGU, Zhang et al. 2020; 3G9W, Anthis et al. 2009), including the structure used in this study: 6VGU (figure 2).

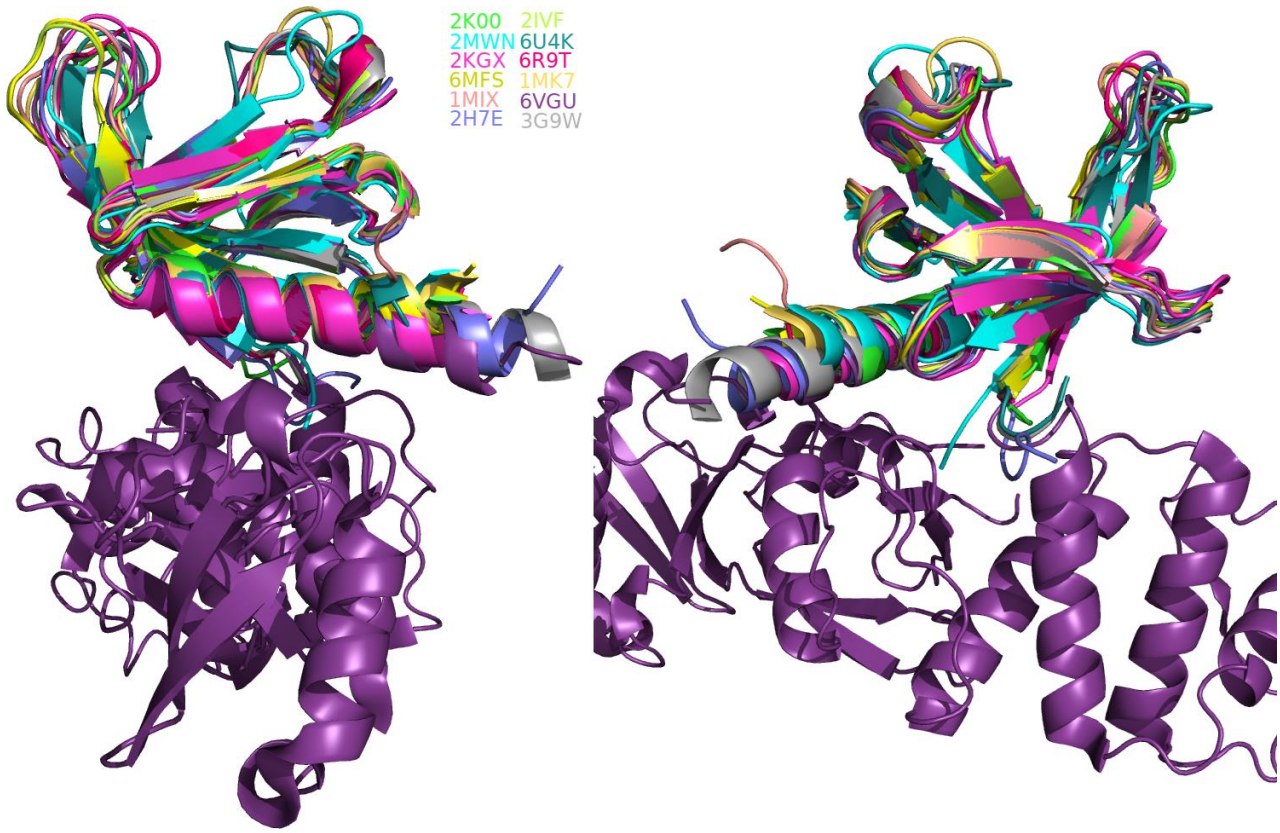

Figure 2. Talin F3 subdomain superposition ("front" view, right, and "side" view, left). The talin-integrin structure used in the current study was based on the PDB structures 6VGU and 2H7E.

(S)MD simulation studies usually start with equilibration MD simulations, which assure that the structural conformation is in a potential energy state that is as low as possible. Without this step, the protein might undergo unwanted movement during the SMD simulation because the initial potential energy would turn into kinetic energy. The structural products of the equilibration MD simulations are used as starting structures for the production of (S)MD simulations.

MD simulation involves the calculation of a trajectory based on Newton's laws of motion: molecular mechanics (MM) or quantum mechanics (QM). QM is usually applied if the binding and unbinding of covalent bonds are involved. QM is not applied in my study because it would make the simulations prohibitively long. MM involves the integration of forces at very short time steps (e.g., 1 femtosecond) and is thus numerical, not analytical. The atomic coordinate file (usually of a protein) that is determined, e.g., by X-ray crystallography, is the basis for the calculation. Even though supercomputers are used for calculations and the computing power has evolved greatly, the simulations are limited by

time. My system took 24 hours of computing time for every 200 ns of simulation using 2 nodes each containing 128 processors at CSC supercomputer Mahti.

Additional force constraint is used in steered molecular dynamics (SMD) simulations. The type of force application is either constant velocity pulling or constant force pulling. In constant velocity pulling (incorporated in my study) a virtual point is placed at the center of a selected atom group or, more often, at the center of two atom groups that are pulled in opposing directions. The virtual point moves at constant velocity and a virtual spring between the point and the atom groups pulls the selected atom group. The spring exerts stronger force as the point gets further away from the atom group. The analysis data generated by constant velocity pulling SMD is a pulling force versus time graph.

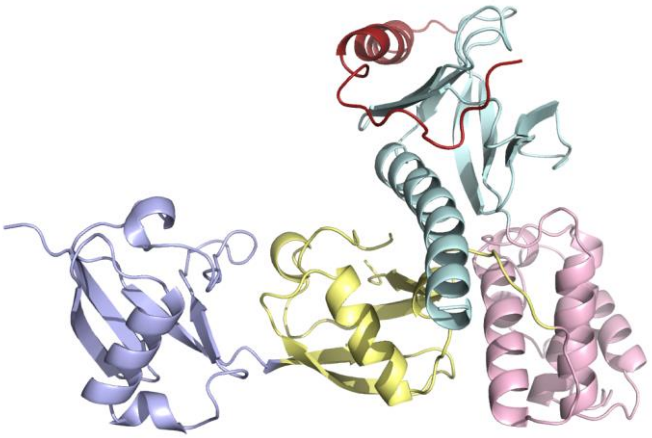

Figure 3. Starting structure used in the simulation. The structure was built using 6VGU and 2H7E as the initial starting point. Coloring of the talin domains: F0 blue, F1 yellow, F2 pink, F3 cyan and the bound integrin peptide is shown in red

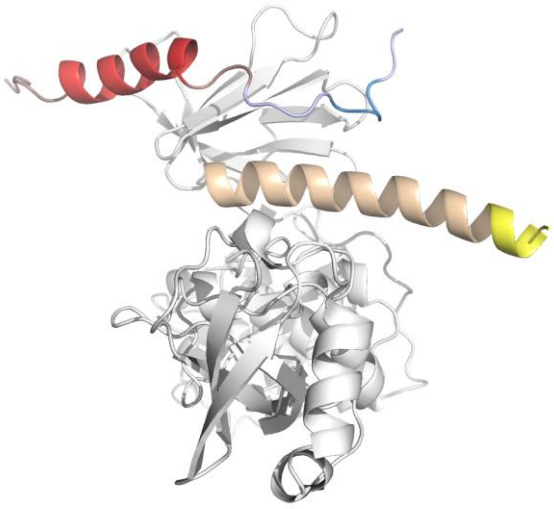

Figure 4. Starting structure (6VGU and 2H7E). Coloring of the features of interes: segment from 2H7E (red), membrane proximal helix (deep red), membrane distal segment (blue), NPLY motif (deep blue), talin C-terminal helix (yellow), and manually appended C-terminal talin residues (deep yellow).

Figure 3 depicts the subdomains of the talin FERM domain and Figure 4 depicts several features of interest in talin: C-terminal helix (residues 385-411), which contains polylysine motif (residues 401-406) and manually modeled terminal residues (407-411); and in integrin: residues modeled according to PDB structure 2H7E (716-739), which contains the membrane proximal helix, and residues modeled according to the PDB structure 6VGU (740-750), which contains the PTB binding NPLY motif. Truncated talin (401-400) is known to have decreased integrin activation compared to talin 401-405, which contains the poly-lysine motif. We had a hypothesis that even longer talin (401-411) might affect the interaction between talin and integrin (unpublished data) and we thus modeled the extra residues to the talin C-terminus based on the predicted secondary structure. Even though we predicted that all the residues in talin head C-terminus (401-411) would adopt an alpha-helix secondary structure, there is opposing evidence that these residues would adopt disordered conformation (García-Alvarez et al. 2003). Several proteins containing the PTB domain (such as talin) bind integrin (Calderwood et al. 2003), but only talin is known to activate integrin (Calderwood et al. 2002). All the PTB proteins bind near the NPLY motif of integrin, but apparently only talin binds the membrane proximal segment of β-integrin, which disrupts integrin α-β interaction and leads to the opening of integrin α-β angle. This in turn propagates to the ectodomains and changes their conformation to an 'opened' form (Wegener et al. 2007).

2 AIMS OF THE STUDY

2.1 How the proposed study and methods relate to past research

Inside–out signaling, in which the association of talin and integrin's cytoplasmic tail domain activates integrin's extracellular domain, and outside–in signaling, in which the association of the ECM ligand and integrin's extracellular head domain activates integrin's cytoplasmic tail domain, have been studied with molecular dynamics (MD) simulations. Although Mehrbod et al. (2013) shed light on some molecular mechanisms involved in both types of activation, the full conformational changes that would explain both activation mechanisms remain unknown. In that research, the molecular structures of integrin and talin were prepared using multiple PDB structures and the talin–integrin interface was determined by MD simulations. However, talin's conformation may not represent the in vivo conformation.

The talin–integrin interface was studied under mechanical tension based on a crystal structure (PDB ID 1MK7), which, encompassing the interaction of talin and integrin, should better represent the interface in vivo (Kukkurainen et al. 2014). In that study, however, talin contained only the F2–F3 segment of the FERM domain, and the talin–integrin interface was presumably not the physiological one, because integrin's NPLY motif did not interact properly with talin's PTB domain; this may have resulted from the molecular design behind the protein construct (fusion protein with potential constraints).

2.2 Research question and hypothesis

Following the previous work, my research question concerns the interaction of the F2–F3 segment of talin-1's FERM domain and integrin β3's cytoplasmic domain (Kukkurainen et al. 2014). However, instead of the PDB structures used in the previous study, I use a recently determined talin-1–integrin β3 complex (PDB ID 6VGU; Zhang et al. 2020), the first and thus far only structure with the arguably native FERM-like domain arrangement of talin-1. Also, the cytoplasmic segment of integrin β3 is presumably in its native binding conformation with, for example, its NPLY motif clearly bound in talin-1. From another PDB structure

(2H7E), membrane-proximal integrin β3 is adopted to the segment of 6VGU integrin β3. Furthermore, my research group is eager to study the contribution of C-terminal talin residues 405-411 for the binding between talin, because those have been shown to enhance integrin activation in previous research (Wehrle-Haller, unpublished data). From there, the research will involve SMD simulations of the complex and analysis of how well the interaction tolerates mechanical tension.

The preliminary research question of the thesis is as follows: How does the talin–integrin interface respond to mechanical tension? The hypothesis is that the interaction is relatively strong, probably stronger than previously reported (Kukkurainen et al. 2014). Hypotheses formulated when initial results have been already acquired include: Does the pulling force profile reveal multiple energy barriers or is there only one cumulative tension? Does the reversed unbinding process reveal a similar binding process, as described earlier?

3 MATERIALS AND METHODS

3.1 Atomic structure preparation

The atomic structures for the proteins used in the study were acquired from Protein Data Bank and modeled by hand with PYMOL. The structure with PDB ID 6VGU contains a talin1 head, a FERM domain, residues 1-406, (excluding F1 flexible loop) complexed with the cytoplasmic membrane distal portion of integrin beta3 (residues 740-750). The integrin cytoplasmic membrane proximal portion (residues 716-739) was adopted from a structure with PDB ID 2H7E. The two portions of integrin were attached manually with PYMOL. Moreover, PYMOL was used to add six additional residues to the C-terminal helix at the end of the talin construct used in the study. Those residues were found to adopt alpha-helical conformation with a secondary structure prediction tool.

3.2 Simulation system preparation

The simulations were conducted with GROMACS. The protein complex, discussed above, was first placed into a dodecahedral simulation box with 1 nm minimal distance from the protein to the sides of the box. An Amber14SB force field was used with SPCE explicit water

molecules. A physiological concentration of salts was achieved by replacing water molecules with K+ and Cl- ions with a concentration of 0.15 M. The system was neutralized by further adding a few ions.

Three short GROMACS runs were used to minimize the energy, equilibrate the temperature, and equilibrate the pressure of the system. The energy minimization was achieved in either the maximum number of 50,000 steps or stopped if the maximum force went below 1000 kJ/mol/nm. The temperature equilibration was also done in 50,000 steps and the temperature of the system was set to 300 K. The protein position was restrained. Pressure equilibration was done in 1,000,000 steps (2 ns with a time step of 2 fs) and the protein position was also restrained. The pressure was maintained at 1 bar using a Parrinello-Rahman barostat (Parrinello & Rahman, 1980; Parrinello & Rahman, 1981).

3.3 Unconstrained equilibrium MDs

Before SMD simulation the talin-integrin complex, as prepared as discussed above, was equilibrated for 200 ns (with a time step of 2 fs); five independent non-constrained MD replicase were performed.

3.4 SMD simulations

For all equilibration and SMD runs periodic boundary conditions were used to imitate an infinite system, in which the atoms appear from the other side of the box when those reach the edge on the other side in all three dimensions (xyz). A V-rescale thermostat (Bussi et al. 2007) was used for temperature coupling by having two separate heat baths for protein and non-protein atoms, with a time constant of 0.1 ps and reference temperature of 300 K. Parrinello-Rahman barostat (Parrinello & Rahman, 1980; Parrinello & Rahman, 1981) was used for pressure coupling with a time constant of 5 ps and reference pressure of 1 bar. The Particle Mesh Ewald method was used for the calculation of coulombic interactions with Fourier spacing of 0.12 nm and interpolation order 4. The coordinates of the whole system were saved every 10 ps.

For all five SMD simulations the products of the five equilibration runs were used as starting structures. The structures were first aligned using GROMACS editconf, -princ, and VMD commands so that the pulling atoms oriented along the z-axis, which was used for pulling.

The pulling atoms were the N-terminal C-alpha of integrin (X716) and the C-terminal C-alpha of talin (X411). The simulation box creation, solvation, ionization, and the three short equilibration runs were conducted similarly to those described above for the 200 ns equilibration MD simulations. The constant velocity pulling speed was set to 0.05 nm/ns and the spring constant to 1000 kJ mol-1 nm-1. The SMD simulation was run for 200-300 ns. The pulling force and the atomic coordinates of the whole system were saved for every 10 ps.

3.5 Three ways to analyze integrin-talin interaction with SMD simulation

Three types of analysis were conducted using PYMOL, VMD and a custom-made plotting software. First, the unbinding and unfolding of talin and integrin were characterized. Six points of interest were chosen from the pulling force profile: before, at the peak and after the first and second peak. The figures were analyzed visually at these six points.

Second, four pairs of amino acids interacting between integrin (D723, F730, W739, Y747) and talin (K318, K324, K357, R358) were chosen based on their importance as discussed in the literature (D723, W739: Mehrbod et al. 2017; F730: Wegener et al. 2007; Y747: Blystone et al. 1997; K318, K324: Zhang et al. 2016; K357: García-Alvarez et al. 2003; R358: Klapholz & Brown, 2017). With the plotting software I specifically made for my analysis the interaction was plotted based on binary decision: the distance between the amino acid (center of mass) pair is below 1 nm.

Third, seven amino acid pairs were found to form hydrogen bond lasting at least 20 % of the total 200 ns of equilibrium MD simulation. The criteria for hydrogen bonding was that the distance between donor and acceptor is no more than 3.5 Å and the angle of the bond is no more than 30 degrees. The amino acid pairs with hydrogen bond lifetime of 20% were determined with VMD and GROMACS hydrogen bonding tool was used to determine the on/off value at specific time points. Those amino acid pairs were also plotted with the custom-made software.

4 RESULTS

4.1 Equilibration MD

The effect of the equilibration of the structure in MD simulations was determined by visual analysis of the superposed initial and final frames of the simulations (Figure 5, see also Appendix 1). The structures were superposed by C-alpha atoms of talin residues 310-400, which correspond with the F3 subdomain. The integrin, which binds to the talin F3 subdomain, is thus also quite well superposed. There were a few differences between the initial and final frames: in all of the five simulations, talin opened from the F2-F3 hinge so that, while F3 was well superposed, the rest of the subdomains were increasingly less superposed after the simulations. In the F3 subdomain the C-terminal helix folded against the bulk of F3 in two of the five simulations. The same helix uncoiled a few residues in three of the five simulations. In all five simulations, integrin was very well superposed at the NPLY motif (residues 744-747) and well aligned at the C-terminal end of the membrane proximal helix. In contrast, the segment between the membrane proximal helix and NPLY motif did not superpose; neither did the N-terminal end of the membrane proximal helix.

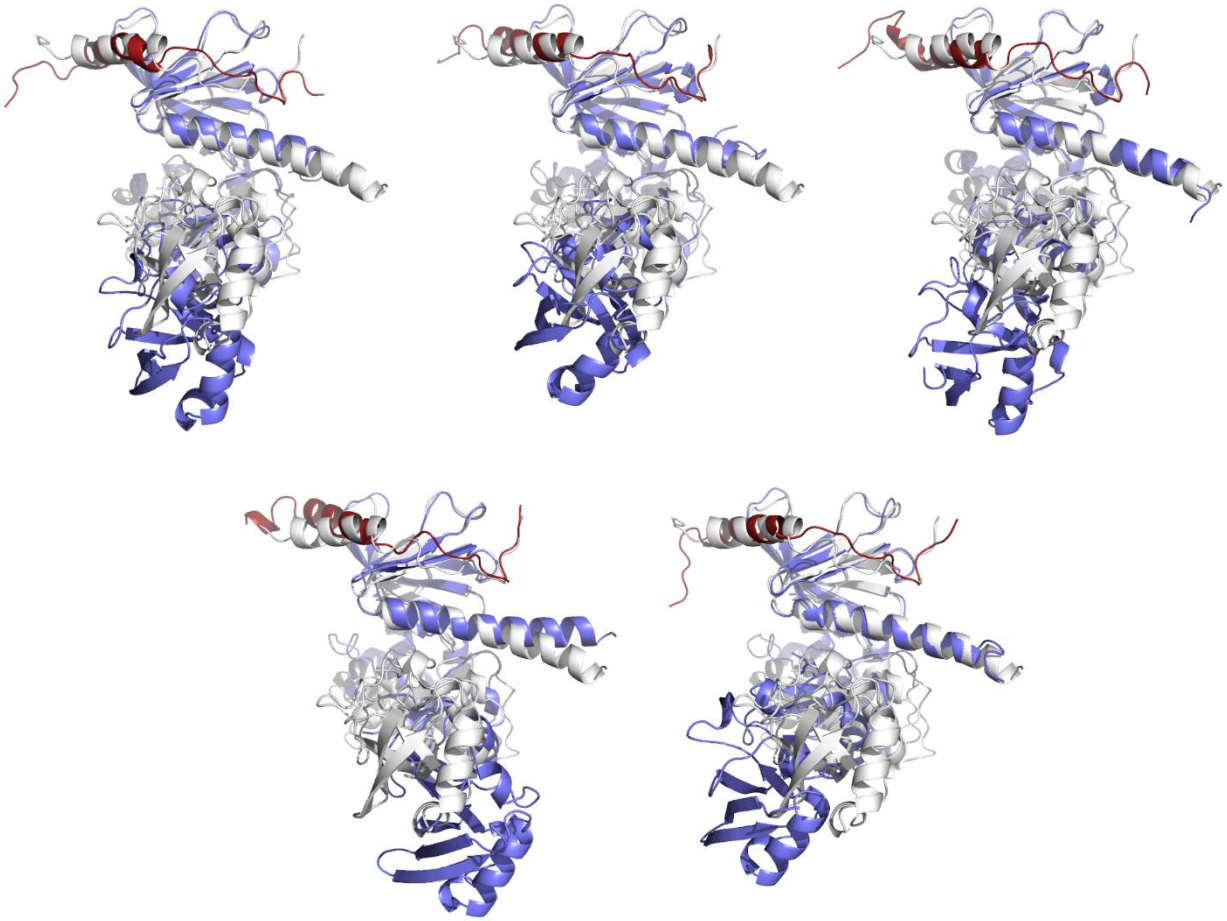

Figure 5. Superposition of the structure snapshots before (white) and after (red integrin and blue talin) the equilibration (replicas 1-5)

4.2 Visualization of the unbinding and unfolding process

The primary focus of my study was the evolution of integrin-talin interaction features as determined by SMD simulation. A constant velocity SMD run produced a pulling force profile as an output. Four out of five of the SMD simulations yielded similar force profiles, with two primary force peaks (Figure 6 shows the SMD run 2 force profile as an example); the remaining one had three peaks. Six points of interest were chosen from the pulling force profiles with two peaks: before the first/second peak, which correspond to the start of higher resistance to pulling; at the first/second peak, which correspond to the local maximum of resistance to pulling; and after the first/second peak, which correspond to the release of the higher resistance to pulling. After the second peak also corresponds to the final release of interaction between talin and integrin.

Structural snapshots revealed the unfolding and unbinding processes (see the detailed structural snapshots in Appendix 1 at the six points of interest marked in Figure 6 of the SMD runs with two peaks). The main events during the four SMD runs are summarized in Table 1.

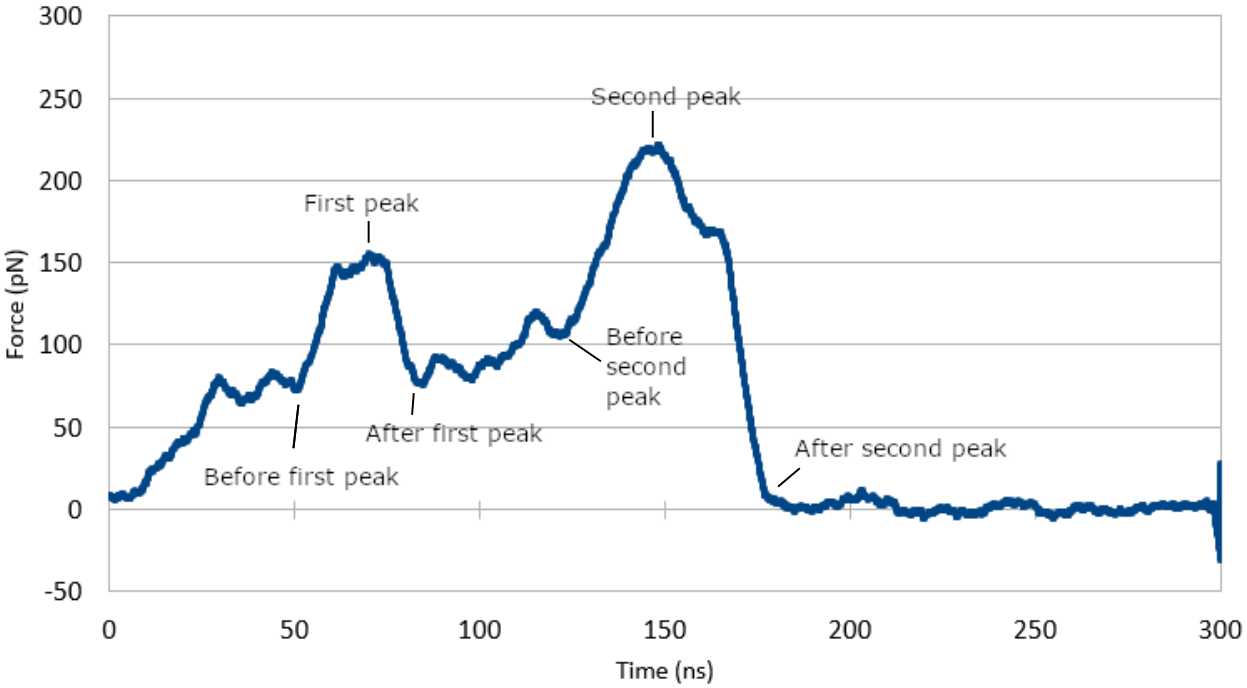

Figure 6. Pulling force profile, SMD run 2, with a moving average of 1000 samples. Four of the five SMD runs contained a similar profile with two force peaks.

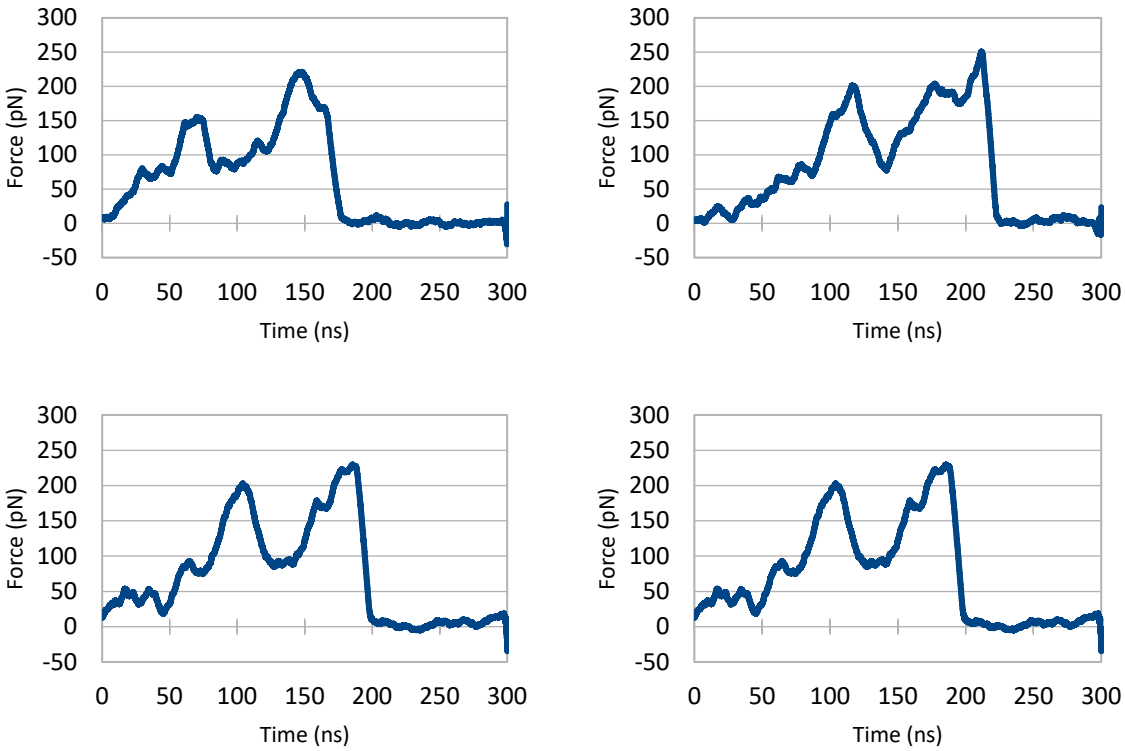

Figure 7. Pulling force profile in all four analyzed SMD replicates (2, 3, 4, and 5).

Figure 8 shows the snapshots at the times of interest for SMD run 2. Compared to the before equilibration MD snapshot (purple), all of the during SMD snapshots (or after the equilibration MD snapshots) had a similar hinge angle at the F2-F3 interface so that talin F1-F2-F3 superposed better in those snapshots. Similarly, all of the during SMD snapshots (except the ending snapshot, red) superposed better in the integrin segment starting after the membrane proximal helix. Yet another effect of equilibration MD is that the F3 C-terminal helix unfolded at residues 408-HFGL-411 (compare purple and blue). However, an opposing effect of equilibration MD was that the integrin membrane proximal helix had two more residues coiled to helix 723-DR-724 (compare purple and blue). Those two residues, however, already unfolded at the *before the first peak* snapshot (red). Another effect of those first 51 ns was that the F3 C-terminal helix unfolded at 405-SKD-407. The same helix unfolded at the poly-lysine segment 401-KKKK-404 by the time of the *at first peak* snapshot and no more unfolding happened at the F3 C-terminal helix during the 300 ns SMD simulation. A major change at the *after the first peak* snapshot was the unbinding of the integrin membrane proximal helix (green). The most C-terminal amino acid of integrin that unbinds at this moment is R736. No unfolding of the integrin membrane proximal helix (725-KEFAKFEEERA-735) happened until the *before the second peak* snapshot, when the only

lasting helix was 730-FEE-732 (yellow). At the *second peak* snapshot integrin unbound few residues – the most N-terminal amino acid that remained bound was W739 (orange). 739-WDTANNPLYKEA-750, the final residues between talin and integrin, unbind only just before the *after the second peak* snapshot.

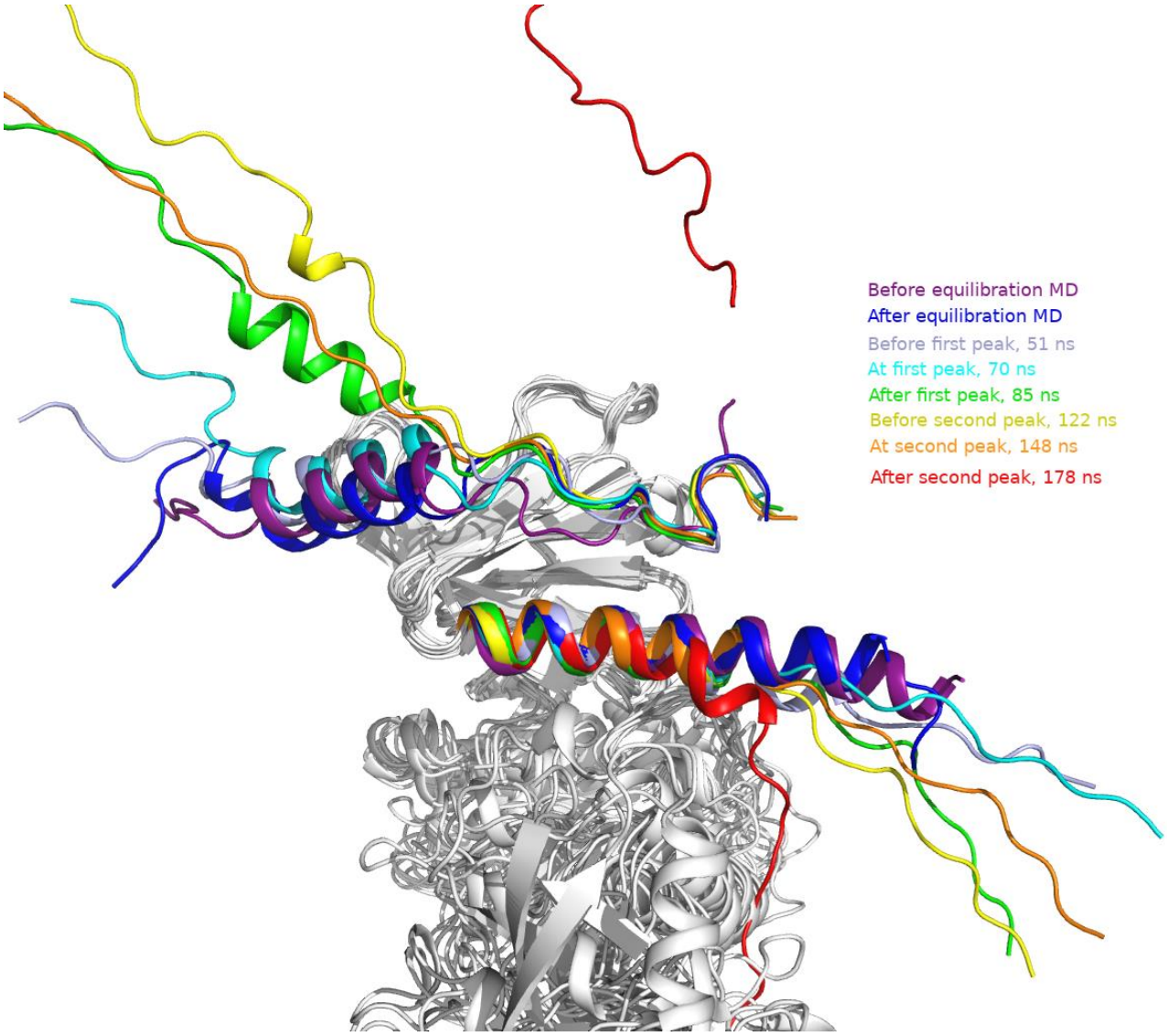

Figure 6. SMD run 2 snapshots. The integrin peptides (upper) and talin C-terminal segments (lower) are colored based on the phase of the SMD run as indicated in the colored labels. The times for the labels are acquired from the pulling force profile (see figures 6 and 7). During the SMD run, integrin N-terminal residue (right) is pulled in the opposing direction of talin C-terminal residue (left). As the SMD proceeds from 0 to 178 ns the integrin peptides dissociate from the talin F3 subdomain, gradually starting from the integrin membrane proximal helix and finally from the area near the NPLY motif.

Figure 9 shows the snapshots at the times of interest for SMD run 3. The F2-F3 hinge opens during the equilibration run similar to run 2 described above, but during SMD simulation the angle breathes more so that *after the first peak* the angle closed back to the initial state.

Also similar to run 2 is that the membrane distal segment of integrin changed conformation during the equilibration run and the conformation stayed the same during the SMD until the *at the second peak* snapshot (magenta), when only 747-YKEA-750 of integrin binds talin. Yet another similarity to the equilibration MD run 2 is that the F3 C-terminal helix unfolded at residues 408-HFGL-411; however, this time the helix folded against the bulk of the F3 subdomain, yet folded back to the original orientation by the time of the *before the first peak* snapshot. Further unfolding of the F3 C-terminal helix happened so that 404-KSKD-407 unfolded by the time of the *before the first peak* snapshot. By the time of the *at the first peak* snapshot the same helix unfolded at 400-LKKK-403. Yet further unfolding of the helix happened at the *at the second peak* snapshot when internal residues 393-AGY-395 unfolded. At the same snapshot half of the helix folded against the bulk of the F1 subdomain. This time integrin membrane proximal helix already unfolded completely at the *after the first peak* snapshot. Integrin membrane distal segment 744-NPLYKEA-750 stayed bound until the time of the *after the second peak* snapshot.

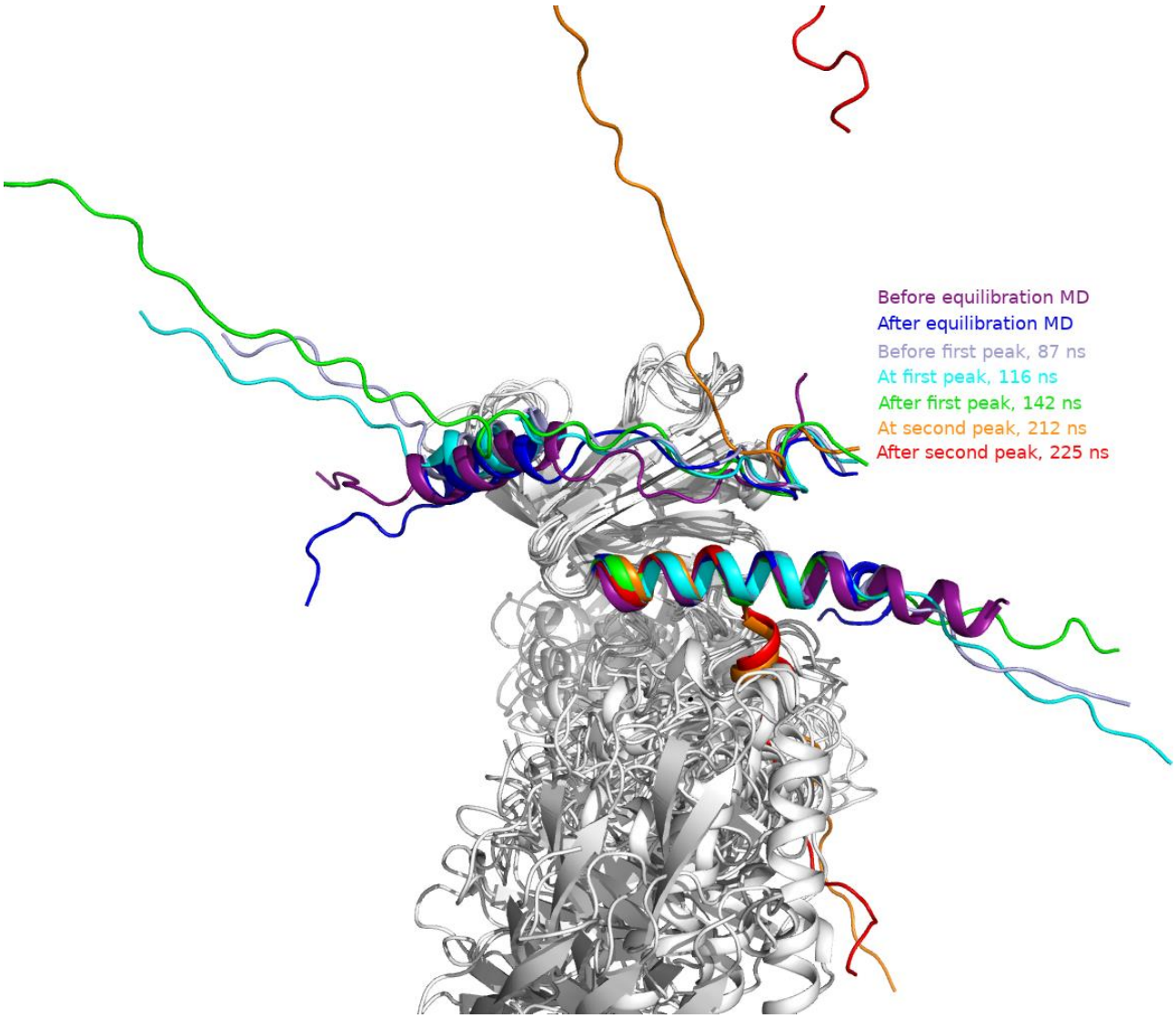

Figure 9. SMD run 3 snapshots

Figure 10 shows the snapshots at the times of interest for SMD run 4. The F2-F3 hinge opens during the equilibration run similarly to runs 2 and 3, and the angle fluctuates similarly to run 3 so that the angle closed to the initial state during the SMD. Similar to runs 2 and 3, the integrin membrane distal segment changes conformation during equilibration run 4 and stays relatively unchanged until *after the first peak* snapshot, when the integrin unbound C-terminally from N743. The integrin remained bound to talin at residues 744-NPLYK-748 until the *at the second peak* snapshot. In the equilibration run 4 the talin C-terminal helix unfolded a little more than in runs 2 and 3, at residues 403-KKSKDHFGL-411. The helix unfolded further during the SMD so that in the final snapshot, *after the second peak*, the helix unfolded at residues 401-KK-402. Similar to SMD run 3, the integrin membrane proximal helix already uncoiled completely at the *after the first peak* snapshot.

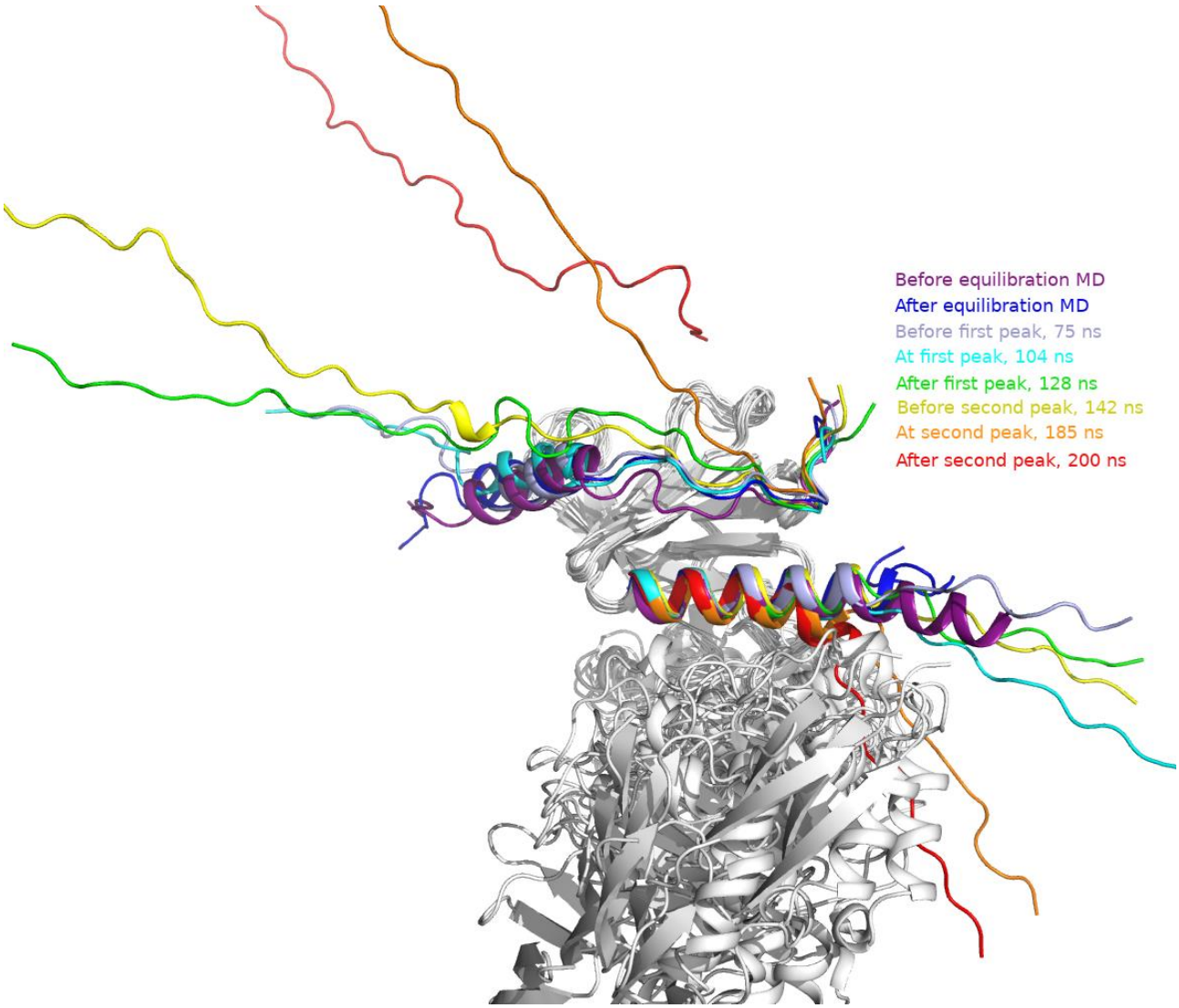

Figure 10. SMD run 4 snapshots

Figure 11 shows the snapshots at the times of interest for SMD run 5. Similar to all the previous runs, the F2-F3 hinge angle opens during the equilibration run 5. Similar to runs 3 and 4, the F2-F3 hinge angle breathed during the SMD run 5 so that the talin conformation was in a comparable state in the *before the second peak* snapshot as it was in the *after the equilibration MD* snapshot. The F1 C-terminal helix uncoiled during the equilibration at residues 407-DHFGL-411 and uncoiled further during the SMD so that it uncoiled at residues 401-KKKKSK-406 by the time of the *before the first peak* snapshot and at residues 394-GYIDIIL-400 by the time of the *at the second peak* snapshot. Similar to all the previous equilibration runs, the integrin segment between the membrane proximal helix and the 744-NPLY-747 motif adopted different conformation that stayed the same until the *before the second peak* snapshot, when the segment started to dissociate from talin. Unlike in SMD runs

2 and 4, where the 744-NPLY-747 segment remained bound in the *at the second peak* snapshot, the segment dissociated comparably to run 3 by that moment.

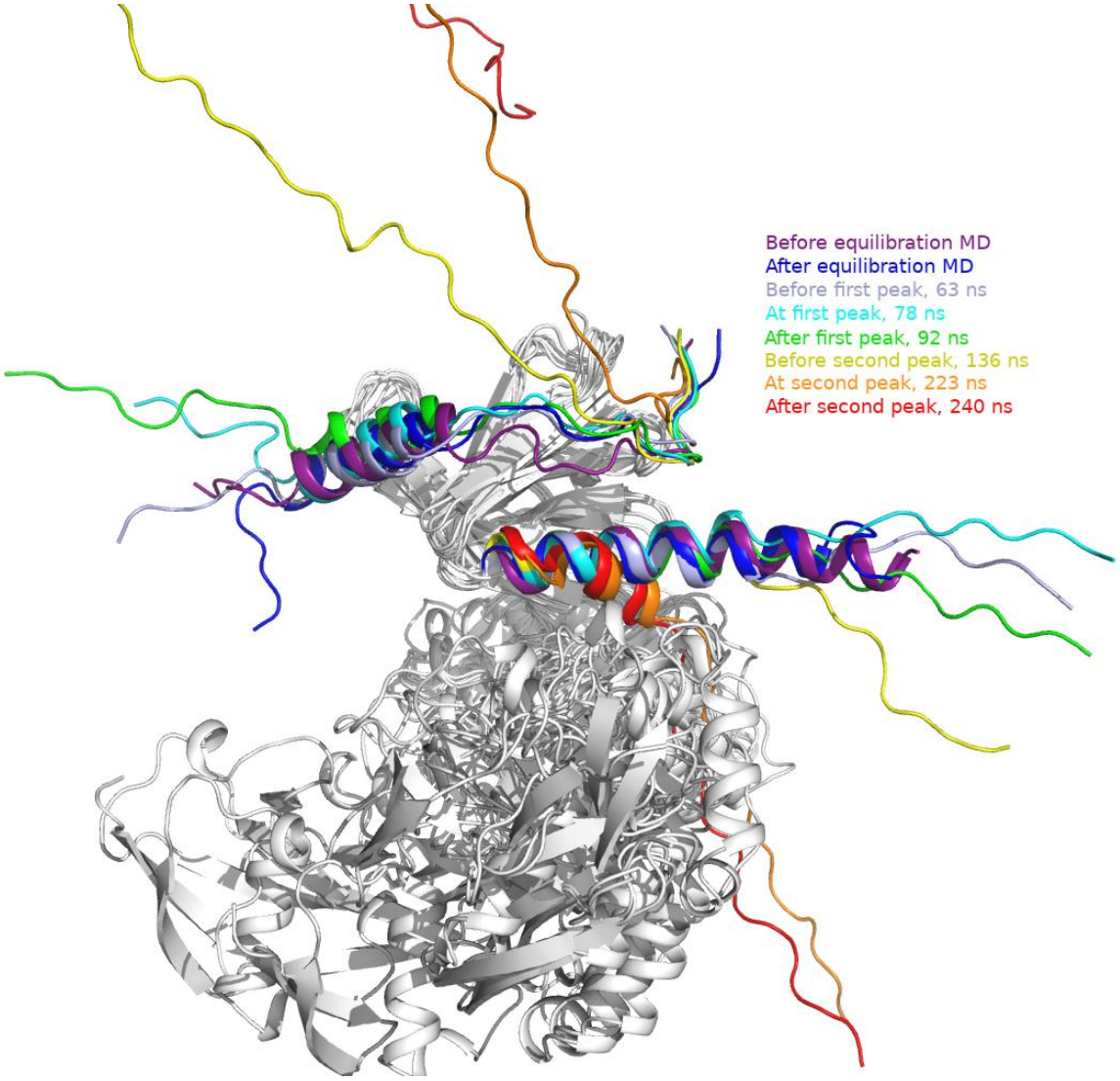

Figure 11. SMD run 5 snapshots

TABLE 1. Summary of SMD unbinding and unfolding events

	SMD run 2	SMD run 3	SMD run 4	SMD run 5
F2-F3 hinge angle	Opens during eq. run and stays the same during SMD	Opens during eq. run and breathes during SMD	Opens during eq. run and breathes during SMD	Opens during eq. run and breathes during SMD
Talin F1 C-terminal helix final uncoiling	Residues 401-411	Residues 393-411	Residues 401-411	Residues 394-411
Integrin membrane-proximal helix uncoiling	After dissociation from talin F3	Before dissociation from talin F3	Before dissociation from talin F3	Before dissociation from talin F3
Integrin residues between membrane-proximal helix and NPLY-motif	Adopts different conformation during eq. run, which stays the same until the *after the second peak* snapshot	Adopts different conformation during eq. run, which stays the same until the *at the second peak* snapshot	Adopts different conformation during eq. run, which stays the same until the *after the first peak* snapshot	Adopts different conformation during eq. run, which stays the same until the *before the second peak* snapshot
Integrin 744-NPLY-747-motif unbinding from talin F3	After the second peak	At the second peak	After the second peak	At the second peak

4.3 Distance of selected amino acid pairs between talin and integrin

A distance analysis was done on four selected amino acid pairs between talin and integrin (Figure 12). The amino acids chosen for the analysis were previously shown to be important for the interaction between talin and integrin: D723 of β3 integrin was shown to interact with the integrin α chain, and the talin mediated rupture of this interaction initiated the dissociation of the two integrin chains and the activation of the integrin extracellular ligand binding head. F730 of integrin penetrated the talin hydrophobic pocket in the integrin membrane proximal helix. Likewise, W739 formed an extensive hydrophobic contact in-between the membrane proximal and membrane distal parts of the integrin. Y747 of integrin was part of the NPLY motif and its significance in talin binding was shown by mutagenesis (Tadokoro et al. 2003). The associated talin amino acid residues were chosen to be the closest amino acids to the selected integrin residues.

To determine if the amino acid pair was interacting, a distance of 1 nm was chosen as a threshold value under which the two amino acids were chosen to be interacting with each other. The amino acid interaction plot (Figure 12) was compared to the pulling force profiles to see if an amino acid pair had a significant force-bearing role in integrin and talin

interaction (Figure 7) - the major interest being the peaks that might correlate between the times of dissociation of the amino acid pair interactions.

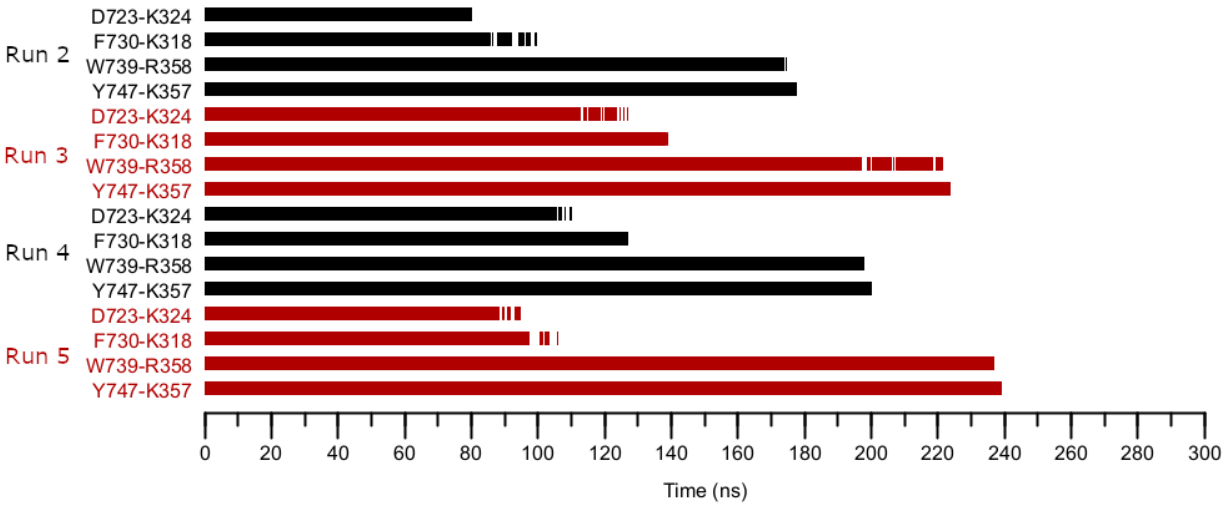

Figure 12. Distance analysis on four amino acid pairs known for their importance in the four analyzed SMD runs. The column represents bound state versus time. The amino acid pair was chosen to be binding if the distance between them was less than 1 nm. The alternating red and black coloring was used to improve the readability.

The dissociation of the D723-K324 amino acid pair happened just after the first peak (runs 2 and 5) and at the top of the first peak (runs 3 and 4). The dissociation of the F730-K318 amino acid pair happened just after the first peak in all four analyzed runs (runs 2, 3, 4, and 5). The dissociation of the W739-R358 amino acid pair happened just before the end of the second peak (runs 2, 4, and 5) and just after the second peak (run 3). The dissociation of the Y747-K357 amino acid pair happened just after the second peak in all four analyzed runs (runs 2, 3, 4, and 5).

4.4 Hydrogen bonds between talin and integrin

Seven pairs of amino acids were chosen for hydrogen bonding analysis (Figure 13). To decide on these pairs the occupancies of all hydrogen bonds in equilibration MD runs (runs 1, 2, 3, 4, and 5) were determined with VMD hydrogen bond analysis, which yielded over 200 hydrogen bonds per equilibration MD run. From these 200+ hydrogen bonds, only those that had an occupancy of more than 20% in at least 4 of 5 equilibration MD runs were chosen for further analysis (which yielded the final 7 pairs).

The unbinding of the hydrogen bond Lys324side-Asp723side correlates with the first energy barrier or pulling force peak. In SMD run 2, it unbinds just after the first peak, but in SMD

run 3 it unbinds just before the first peak; in SMD runs 4 and 5 it unbinds at the highest points of the first peak.

The unbinding of the hydrogen bond Ser362side-Glu733side also correlates with the first energy barrier. In all of the analyzed SMD runs (2, 3, 4, and 5) it unbinds just after the first peak.

With one exception (Lys748main-Thr354main in SMD run 4) there are four hydrogen bonds in each of the 4 SMD runs, whose unbinding correlate with the second energy barrier. Asn744main-Lys357main, Asn744side-Ile356main, Asp372main-Tyr747side, and Lys748main-Thr354main all unbind just after the second peak.

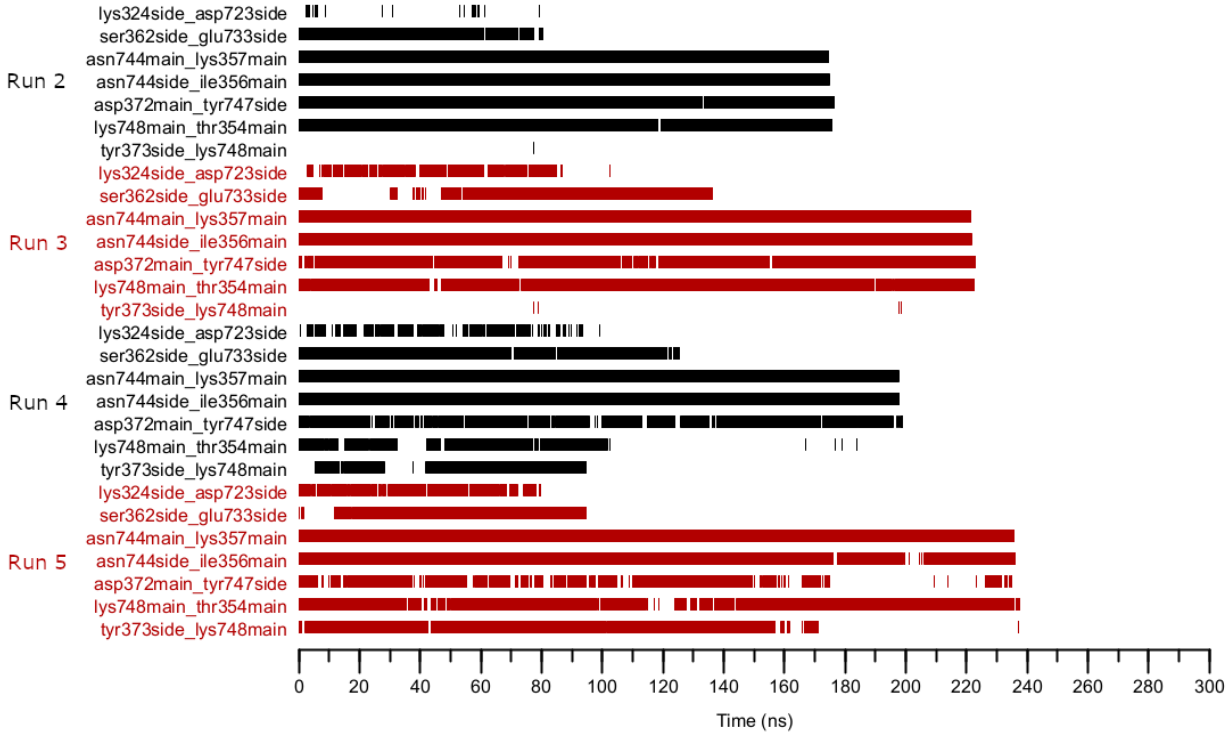

Figure 13. Hydrogen bonding analysis on seven amino acid pairs in the four analyzed SMD replicas. The column represents bound state versus time. Hydrogen bonds were chosen to be active if the following criteria match: distance between the donor and acceptor is less than 0.35 nm and the angle is less than 30 degrees. The alternating red and black coloring is used to improve the readability.

5 DISCUSSION

The interface between talin and integrin under mechanical stress was previously studied (Kukkurainen et al. 2014); although with partially different procedures and different protein coordinate structures, my results will be compared to those where possible. The protein

coordinate files from the PDB database (including talin head-integrin cytoplasmic tail interaction) that they used were 1MK7 (Garcia-Alvarez et al. 2003) and 3G9W (Anthis et al. 2009). 1MK7 contains F2F3 subdomains of talin-1 FERM head and residues 196-400, in complex with integrin beta3 cytoplasmic tail 739-WDTANNPLYKE-750. The talin F2F3 segment was shown to bind and activate integrin as strongly as either the talin F3 or the whole talin head (Garcia-Alvarez et al. 2002). 3G9W also contains the F2F3 segment (residues 198-408), but from talin-2. It also contains a much longer integrin beta1D cytoplasmic tail. Perhaps surprisingly, when trying to crystallize the talin-integrin complex, the binding affinity of the two proteins was found to be relatively weak. Thus, the structure used in my work, 6VGU, and the structure 1MK7 were made possible only by covalently binding integrin and talin together.

It has proven difficult to acquire a complete beta3 cytoplasmic tail in complex with talin in atomic resolution (Wegener et al. 2007; Zhang et al. 2020). Similarly to the structure 1MK7 described above, the 6VGU contained only the membrane distal segment of the beta3 cytoplasmic domain; even though the purified beta3 contained residues 720-750, the crystallized sequence was only residues 741-750, the rest being disordered. We were, however, interested to study the full beta3 cytoplasmic tail, which was made possible by combining structures 6VGU (residues 741-750) and 2H7E (residues 716-739).

As computers (also super-computers) are acquiring increasing processing performance, MD simulations are getting more accurate and longer. Computational studies are thus getting closer to experimental studies in terms of the temporal time window, consequently yielding results that better match *in vivo* conditions. The forces in SMD simulation that have to be used in order to cause the desired unbinding/unfolding event are also getting smaller, which means the simulation contains fewer artifacts caused by non-biologically large forces. The great challenge of (S)MD simulations is to acquire quantitative results instead of qualitative ones. For example, the pulling forces (in constant velocity SMD) and rupture forces (the pulling velocity maximum) in my study are qualitative in nature and thus not really comparable to experimental (atomic force microscopy, AFM) or even other SMD studies. Even though the pulling forces are qualitative they provide meaningful comparison points inside a single SMD study. In the future, the SMD pulling forces and time window may finally match those used in AFM, and the pulling forces can be assumed to be similar in these two kinds of experiments. Even with the high forces and short time periods the

(S)MD simulations yield important information on the atomic binding/folding/unbinding/ unfolding events. The important amino acid residues taking part in interactions can thus be determined and, e.g., used as a guide to construct recombinant proteins with desired properties.

One intriguing possibility of SMD studies is to infer the binding/folding pathway by reversely interpreting the unbinding/unfolding pathway.

5.1 Visual inspection of the unbinding and unfolding process

The inevitable effect of pulling two non-covalently binding proteins is their eventual unbinding. This SMD simulation also resulted in partial unfolding of the talin C-terminal helix. Four out of five of the SMD simulations were included in the analysis; unlike SMD run 1, which was left out of analysis and had three peaks in the pulling force profile, the four others had two peaks in the pulling force profile. Run 1 was defined as an outlier and was left out to make analysis easier. The unbinding of the talin head and integrin tail was thus assumed to be a two-step process, i.e., it had two energy barriers. The initial pulling force profiles were relatively noisy, but a calculation of moving average with 1000 samples revealed the process to have two energy barriers.

The equilibration MD runs had a consistent transformational effect on talin and integrin: talin had a hinge between F2 and F3 subdomains that opened in all equilibration runs. Another effect was that in some of the runs the talin F3 C-terminal helix unfolded up to three residues. Integrin, conversely, had its segment between the membrane proximal part and the NPLY motif translated upwards and remained so in all the SMD runs until the final (*after the second peak*) snapshot.

5.2 Amino acid distance analysis

Residues D723 of integrin beta3 and K324 of talin-1 were shown several times to be an important pair of amino acids in integrin conditional and talin-dependent activation (Hughes et al. 1996). The pair supposedly forms a salt bridge between each other, and *in vivo*, simultaneously breaks an integrin activation-preventing salt bridge between D723 of integrin beta3 and R995 of integrin alphaIIb. Mutation of either one of the integrin alpha or beta residues breaks the salt bridge and generates constitutively, talin-independently, active

integrin (Hughes et al. 1996). It was shown that while expressing wildtype integrin with wildtype talin yields active integrin as expected, expression of K324D mutant talin with wildtype integrin yields inactive integrin (Anthis et al. 2009). Owing to its importance, it was chosen as one of the four amino acid pairs incorporated in the distance analysis.

The unique ability of talin among PTB-containing proteins to activate integrins was investigated by Wegener et al. (2007). They propose that the function of the talin-integrin membrane distal interaction is to form a strong initial linkage between the proteins, and subsequently the interaction between talin and integrin membrane proximal segment results in integrin activation. Based on their atomic resolution structural model of the beta3 membrane proximal segment they figured out important residues of talin and integrin in integrin activation. Two such residues in integrin were F727 and F730, which penetrate into a deep hydrophobic pocket in a mobile loop in talin. The mobile loop contains, among others, residue L325. Indeed, the mutagenesis L325R undoes that pocket and prevents integrin membrane proximal segment binding to talin, which also prevents the talin mediated integrin activation. Other PTB-containing proteins lack that kind of pocket-forming mobile loop (Wegener et al. 2007).

Being in the middle of integrin beta3 cytoplasmic tail, residue W739 of integrin beta3 was incorporated in both membrane proximal (2H7E) and membrane distal (1MK7) integrin beta3 cytoplasmic segments. The importance of this residue in high affinity binding is emphasized by the identical position of Trp in phosphatidylinositol phosphate kinase type Iγ (PIPKIγ) (Wegener et al. 2007). PIPKIγ is another protein that binds the integrin beta3 cytoplasmic tail membrane distal segment. The higher affinity of PIPKIγ to integrin beta3 than talin F3 allowed the determination of the beta3 membrane proximal segment by formation of the beta3 membrane proximal segment-PIPKIγ membrane distal segment chimera, as proven in the structure 2H7E (Wegener et al. 2007).

The final amino acid pair used in the distance analysis included Y747 and K357. The tyrosine is contained within a 744-NPLY-747 (integrin beta3) motif that was implicated in a variety of roles, especially in cell surface receptors. In an early database search-based investigation, Chen et al. (1990) found that NPXY is found in the cytoplasmic side of several cell surface receptors much more often than could be explained by pure chance. They demonstrated that the NPXY motif is essential in the endocytosis of low-density lipoprotein receptor and proposed a similar function for other cell surface receptors. Particularly, they pointed out

that the Tyr of NPXY is the most essential of the amino acids in NPXY recognition and that the remaining three amino acids merely provide a proper context for the Tyr-based interaction. Alternatively, NPLY of integrin of beta3 was shown not to be essential in the endocytosis of αIIbβ3 (Ylänne et al. 1995). However, they demonstrated the significance of Y747 in the cell spreading mediated by αIIbβ3. More recently it was shown that Y747 is critical in the binding of paxillin and possibly other signaling proteins that mediate cell spreading, and not in the binding of talin or in the formation of focal adhesions (Pinon et al. 2014).

5.3 Hydrogen bond analysis

To get further precise information about the unbinding events between talin and integrin, the binding/unbinding graph in the different SMD runs was prepared with all the hydrogen bonds that had occupancies of 20% or more in the equilibration replicas (seven in total). The residues that belong to integrin in hydrogen bonds Lys324-Asp723 and Ser362-Glu733, are part of the membrane proximal helix. Their unbinding correlate with the first energy barrier. Likewise, the unbinding of four hydrogen bonds that had residues belonging to the membrane distal part correlates with the second energy barrier. A previous study that investigated hydrogen bond lifetimes between talin and integrin uncovered altogether different hydrogen bonding pairs (Kukkurainen et al. 2014). Four of their longest-lasting hydrogen bond pairs were Q734-W359 (84%), T737-K357 (66.7%), A361-K732 (62%), and W359-T735 (62%).

6 CONCLUSIONS

The results reveal a two-step process of talin-integrin dissociation in which major energy barriers in pulling force profiles correlate with 1) the unbinding of integrin membrane proximal helix from talin, and 2) the unbinding of membrane distal segment or NPLY motif from talin. The hypothesis that the pulling force profile contains multiple peaks is thus supported. The other hypothesis is also supported; the reversed unbinding process, which approximates the binding process, is similar to what was previously observed (García-Alvarez et al. 2003). The NPLY motif of integrin first binds to talin, which is followed by the

binding of the integrin membrane proximal segment. The latter binding is associated with the simultaneous formation of helix conformation. The observed binding process might, however, be the result of the steering force directions. Answers to the preliminary hypothesis were, however, unfortunately not acquired because the methods chosen in the current study and the previous study were significantly different (Kukkurainen et al. 2014). However, their finding that the NPxY motif play a minor role in the force resistance between talin F3 and beta integrin cytoplasmic tail differs from my finding that it might actually play a significant role in the binding of these two proteins. Also, this study revealed no significant role for talin C-terminal residues 405-411 in the interaction between talin and integrin beta3 tail. Further study about the significance of these residues would involve a comparison of structures that contain these residues and structures with those that do not contain these residues. This is the second study to investigate beta integrin cytoplasmic tail binding with talin F3 subdomain with SMD (Kukkurainen et al. 2014). However, this is the first such study that incorporates the full cytoplasmic tail with the (presumably) authentic FERM-folded talin head domain (Zhang et al. 2020). The acquired data reveal a two-step (un)binding process, in which the first step (or force barrier) is associated with the membrane-proximal segment dissociation and the second step with the dissociation of the membrane-distal segment. As pointed out by Zhang et al. (2020), one relevant direction of study would involve the investigation of the ternary complex between beta integrin cytoplasmic tail, talin head domain, and kindlin, because in vivo talin alone seems to not be enough to activate integrins. It might, e.g., reveal a clue (because of the nature of possible talin head-kindlin interaction) as to why talin head C-terminal helix was observed to be significant in the activation and clustering of integrins (Zhang et al. 2020), which was not observed in the current study.

ACKNOWLEDGEMENTS

I wrote this thesis as an employee of the Protein Dynamics group of the University of Tampere, led by prof. Vesa Hytönen in 2021-2022. In addition to Vesa, I had two other supervisors: prof. Jari Ylänne (University of Jyväskylä) and PhD Vasyl Mykuliak (University of Tampere). The initial idea of the thesis originated from Vesa, and Vasyl was my main support in the day-to-day problems I faced during this project. Because of the coronavirus pandemic, I carried out all of my work remotely in my home and connected with the supervisors via emails and remote online meetings. Although I find the subject matter very interesting, I would have probably benefited from working in the office surrounded by other scientists while modeling and simulating molecular systems with a computer, at least in terms of motivation and learning new things. I am deeply thankful to Vesa and Vasyl for all of their ideas and suggestions during the project. Vasyl was of tremendous help with the details of modeling and simulating the protein systems. I am also thankful to Vesa, Vasyl, and Jari for all the comments on the nearly finished thesis draft.

In Tampere, 24th of November 2022

Lassi Palmujoki

REFERENCES

Alford, A. I., Kozloff, K. M., & Hankenson, K. D. (2015). Extracellular matrix networks in bone remodeling. *The international journal of biochemistry & cell biology*, 65, 20-31.

Allen, M.P., (2004). Introduction to molecular dynamics simulation. *Computational soft matter: from synthetic polymers to proteins*, 23(1), 1-28.

Anthis, N. J., Wegener, K. L., Critchley, D. R., & Campbell, I. D. (2010). Structural diversity in integrin/talin interactions. *Structure*, 18(12), 1654-1666.

Anthis, N. J., Wegener, K. L., Ye, F., Kim, C., Goult, B. T., Lowe, E. D., Vakonakis, I., Bate, N., Critchley, D. R., Ginsberg, M. H., & Campbell, I. D. (2009). The structure of an integrin/talin complex reveals the basis of inside-out signal transduction. *The EMBO journal*, 28(22), 3623–3632.

Atherton, P., Lausecker, F., Carisey, A., Gilmore, A., Critchley, D., Barsukov, I., & Ballestrem, C. (2020). Relief of talin autoinhibition triggers a force-independent association with vinculin. *Journal of Cell Biology*, 219(1).

Bachmann, M., Kukkurainen, S., Hytönen, V. P., & Wehrle-Haller, B. (2019). Cell adhesion by integrins. *Physiological reviews*, 99(4), 1655-1699.

Barnes, J. M., Przybyla, L., & Weaver, V. M. (2017). Tissue mechanics regulate brain development, homeostasis and disease. *Journal of cell science*, 130(1), 71-82.

Block, M. R., Badowski, C., Millon-Fremillon, A., Bouvard, D., Bouin, A. P., Faurobert, E., Gerber-Scokaert, D., Planus, E., & Albiges-Rizo, C. (2008). Podosome-type adhesions and focal adhesions, so alike yet so different. *European journal of cell biology*, 87(8-9), 491-506.

Blystone, S. D., Williams, M. P., Slater, S. E., & Brown, E. J. (1997). Requirement of integrin β3 tyrosine 747 for β3 tyrosine phosphorylation and regulation of αvβ3 avidity. *Journal of Biological Chemistry*, 272(45), 28757-28761.

Bowers, S. L., Banerjee, I., & Baudino, T. A. (2010). The extracellular matrix: at the center of it all. *Journal of molecular and cellular cardiology*, 48(3), 474-482.

Buccione, R., Caldieri, G., & Ayala, I. (2009). Invadopodia: specialized tumor cell structures for the focal degradation of the extracellular matrix. *Cancer and Metastasis Reviews*, 28(1), 137-149.

Burridge, K. (2017). Focal adhesions: a personal perspective on a half century of progress. *The FEBS journal*, 284(20), 3355-3361.

Bussi, G., Donadio, D., & Parrinello, M. (2007). Canonical sampling through velocity rescaling. *The Journal of chemical physics*, 126(1), 014101.

Calderwood, D. A., Fujioka, Y., de Pereda, J. M., García-Alvarez, B., Nakamoto, T., Margolis, B., McGlade, C. J., Liddington, R. C., & Ginsberg, M. H. (2003). Integrin beta cytoplasmic domain interactions with phosphotyrosine-binding domains: a structural prototype for diversity in integrin signaling. *Proceedings of the National Academy of Sciences of the United States of America*, 100(5), 2272–2277.

Calderwood, D. A., Tuckwell, D. S., Eble, J., Kühn, K., & Humphries, M. J. (1997). The integrin α1 A-domain is a ligand binding site for collagens and laminin. *Journal of Biological Chemistry*, 272(19), 12311-12317.

Calderwood, D. A., Yan, B., de Pereda, J. M., Alvarez, B. G., Fujioka, Y., Liddington, R. C., & Ginsberg, M. H. (2002). The phosphotyrosine binding-like domain of talin activates integrins. *Journal of Biological Chemistry*, 277(24), 21749-21758.

Calderwood, D. A., Zent, R., Grant, R., Rees, D. J. G., Hynes, R. O., & Ginsberg, M. H. (1999). The talin head domain binds to integrin β subunit cytoplasmic tails and regulates integrin activation. *Journal of Biological Chemistry*, 274(40), 28071-28074.

Campbell, I. D., & Humphries, M. J. (2011). Integrin structure, activation, and interactions. *Cold Spring Harbor Perspectives in Biology*, 3(3), a004994.

Chan, K. T., Bennin, D. A., & Huttenlocher, A. (2010). Regulation of adhesion dynamics by calpain-mediated proteolysis of focal adhesion kinase (FAK). *Journal of Biological Chemistry*, 285(15), 11418-11426.

Chen, W. J., Goldstein, J. L., & Brown, M. S. (1990). NPXY, a sequence often found in cytoplasmic tails, is required for coated pit-mediated internalization of the low density lipoprotein receptor. *The Journal of biological chemistry*, 265(6), 3116–3123.

Chen, X., Xie, C., Nishida, N., Li, Z., Walz, T., & Springer, T. A. (2010). Requirement of open headpiece conformation for activation of leukocyte integrin αXβ2. *Proceedings of the National Academy of Sciences*, 107(33), 14727-14732.

Cluzel, C., Saltel, F., Lussi, J., Paulhe, F., Imhof, B. A., & Wehrle-Haller, B. (2005). The mechanisms and dynamics of αvβ3 integrin clustering in living cells. *The Journal of cell biology*, 171(2), 383-392.

Das, M., Ithychanda, S., Qin, J., & Plow, E. F. (2014). Mechanisms of talin-dependent integrin signaling and crosstalk. *Biochimica et biophysica acta*, 1838(2), 579–588.

Dedden, D., Schumacher, S., Kelley, C. F., Zacharias, M., Biertümpfel, C., Fässler, R., & Mizuno, N. (2019). The architecture of Talin1 reveals an autoinhibition mechanism. *Cell*, 179(1), 120-131.

Del Rio, A., Perez-Jimenez, R., Liu, R., Roca-Cusachs, P., Fernandez, J. M., & Sheetz, M. P. (2009). Stretching single talin rod molecules activates vinculin binding. *Science*, 323(5914), 638-641.

Debrand, E., Conti, F. J., Bate, N., Spence, L., Mazzeo, D., Pritchard, C. A., Monkley, S. J., & Critchley, D. R. (2012). Mice carrying a complete deletion of the talin2 coding sequence are viable and fertile. *Biochemical and Biophysical Research communications*, 426(2), 190-195.

Elliott, P. R., Goult, B. T., Kopp, P. M., Bate, N., Grossmann, J. G., Roberts, G. C., Critchley, D. R., & Barsukov, I. L. (2010). The Structure of the talin head reveals a novel extended conformation of the FERM domain. *Structure*, 18(10), 1289-1299.

Forman-Kay, J. D. & Pawson, T. (1999). Diversity in protein recognition by PTB domains. *Current opinion in structural biology*, 9(6), 690-695.

Franco, S. J., Rodgers, M. A., Perrin, B. J., Han, J., Bennin, D. A., Critchley, D. R., & Huttenlocher, A. (2004). Calpain-mediated proteolysis of talin regulates adhesion dynamics. *Nature cell biology*, 6(10), 977-983.

García-Alvarez, B., de Pereda, J. M., Calderwood, D. A., Ulmer, T. S., Critchley, D., Campbell, I. D., Ginsberg, M. H., & Liddington, R. C. (2003). Structural determinants of integrin recognition by talin. *Molecular cell*, 11(1), 49–58.

Gough, R. E., & Goult, B. T. (2018). The tale of two talins - two isoforms to fine-tune integrin signalling. *FEBS letters*, 592(12), 2108–2125.

Hill, P. A. (1998). Bone remodelling. *British journal of orthodontics*, 25(2), 101-107.

Goult, B. T., Bate, N., Anthis, N. J., Wegener, K. L., Gingras, A. R., Patel, B., Barsukov, I. L., Campbell, I. D., Roberts, G. C., & Critchley, D. R. (2009). The structure of an interdomain complex that regulates talin activity. *The Journal of biological chemistry*, 284(22), 15097–15106.

Goult, B. T., Yan, J., & Schwartz, M. A. (2018). Talin as a mechanosensitive signaling hub. *The Journal of Cell Biology*, 217(11), 3776–3784.

Haining, A. W., von Essen, M., Attwood, S. J., Hytönen, V. P., & Del Río Hernández, A. (2016). All Subdomains of the Talin Rod Are Mechanically Vulnerable and May Contribute To Cellular Mechanosensing. *ACS nano*, 10(7), 6648–6658.

Hollingsworth, S.A. and Dror, R.O. (2018). Molecular dynamics simulation for all. *Neuron*, 99(6), pp.1129-1143.

Horton, M. A. (1997). The αvβ3 integrin "vitronectin receptor". *The international journal of biochemistry & cell biology*, 29(5), 721-725.

Hughes, P. E., Diaz-Gonzalez, F., Leong, L., Wu, C., McDonald, J. A., Shattil, S. J., & Ginsberg, M. H. (1996). Breaking the Integrin Hinge: A DEFINED STRUCTURAL CONSTRAINT REGULATES INTEGRIN SIGNALING (∗). *Journal of Biological Chemistry*, 271(12), 6571-6574.

Humphries, J. D., Byron, A., & Humphries, M. J. (2006). Integrin ligands at a glance. *Journal of cell science*, 119(19), 3901-3903.

Humphrey, J. D., Dufresne, E. R., & Schwartz, M. A. (2014). Mechanotransduction and extracellular matrix homeostasis. *Nature reviews Molecular cell biology*, 15(12), 802-812.

Hytönen, V. P., & Vogel, V. (2008). How force might activate talin's vinculin binding sites: SMD reveals a structural mechanism. *PLoS computational biology*, 4(2), e24.

Hytönen, V. P., & Wehrle-Haller, B. (2016). Mechanosensing in cell–matrix adhesions – Converting tension into chemical signals. *Experimental Cell Research*, 343(1), 35-41.

Isomursu, A., Park, K. Y., Hou, J., Cheng, B., Mathieu, M., Shamsan, G. A., Fuller, B., Kasim, J., Mahmoodi, M. M., Lu, T. J., Genin, G. M., Xu, F., Lin, M., Distefano, M. D., Ivaska, J., & Odde, D. J. (2022). Directed cell migration towards softer environments. *Nature materials*, 21(9), 1081–1090.

Klapholz, B., & Brown, N. H. (2017). Talin - the master of integrin adhesions. *Journal of Cell Science*, 130(15), 2435–2446.

Krieg, M., Fläschner, G., Alsteens, D., Gaub, B. M., Roos, W. H., Wuite, G. J., Gaub H. E., Gerber C., Dufrêne Y. F. & Müller, D. J. (2019). Atomic force microscopy-based mechanobiology. *Nature Reviews Physics*, 1(1), 41-57.

Kukkurainen, S., Azizi, L., Zhang, P., Jacquier, M. C., Baikoghli, M., von Essen, M., Tuukkanen, A., Laitaoja, M., Liu, X., Rahikainen, R., Orłowski, A., Jänis, J., Määttä, J., Varjosalo, M., Vattulainen, I., Róg, T., Svergun, D., Cheng, R. H., Wu, J., Hytönen, V. P., Wehrle-Haller, B. (2020). The F1 loop of the talin head domain acts as a gatekeeper in integrin activation and clustering. *Journal of cell science*, 133(19), jcs239202.

Kukkurainen, S., Määttä, J. A., Saeger, J., Valjakka, J., Vogel, V. & Hytönen, V. P. (2014). The talin–integrin interface under mechanical stress. *Molecular BioSystems*. 10(12), 3217-3228.

Kääpä, A., Peter, K., & Ylänne, J. (1999). Effects of mutations in the cytoplasmic domain of integrin β1 to talin binding and cell spreading. *Experimental cell research*, 250(2), 524-534.

Lagarrigue, F., Gingras, A. R., Paul, D. S., Valadez, A. J., Cuevas, M. N., Sun, H., Lopez-

Ramirez, M. A., Goult, B. T., Shattil, S. J., Bergmeier, W., & Ginsberg, M. H. (2018). Rap1 binding to the talin 1 F0 domain makes a minimal contribution to murine platelet GPIIb-IIIa activation. *Blood advances*, 2(18), 2358-2368.

Lau, T. L., Kim, C., Ginsberg, M. H., & Ulmer, T. S. (2009). The structure of the integrin alphaIIbbeta3 transmembrane complex explains integrin transmembrane signalling. *The EMBO Journal*, 28(9), 1351–1361.

Lauffenburger, D. A., & Horwitz, A. F. (1996). Cell migration: a physically integrated molecular process. *Cell*, 84(3), 359-369.

Lee, D. A., Knight, M. M., Campbell, J. J., & Bader, D. L. (2011). Stem cell mechanobiology. *Journal of cellular biochemistry*, 112(1), 1-9.

Lu, F., Zhu, L., Bromberger, T., Yang, J., Yang, Q., Liu, J., Plow, E.F., Moser, M. and Qin, J., (2022). Mechanism of integrin activation by talin and its cooperation with kindlin. *Nature communications*, 13(1), 1-19.

Ludwig, B. S., Kessler, H., Kossatz, S., & Reuning, U. (2021). RGD-binding integrins revisited: how recently discovered functions and novel synthetic ligands (re-) shape an ever-evolving field. *Cancers*, 13(7), 1711.

Lund, A. W., Yener, B., Stegemann, J. P., & Plopper, G. E. (2009). The natural and engineered 3D microenvironment as a regulatory cue during stem cell fate determination. Tissue engineering. *Part B, Reviews*, 15(3), 371–380.

Mak, M., Kim, T., Zaman, M. H., & Kamm, R. D. (2015). Multiscale mechanobiology: computational models for integrating molecules to multicellular systems. *Integrative Biology: Quantitative Biosciences from Nano to Macro*, 7(10), 1093–1108.

Maoiléidigh, D. Ó., & Ricci, A. J. (2019). A bundle of mechanisms: Inner-ear hair-cell mechanotransduction. *Trends in neurosciences*, 42(3), 221-236.

Martel, V., Racaud-Sultan, C., Dupe, S., Marie, C., Paulhe, F., Galmiche, A., Block, M. R., & Albiges-Rizo, C. (2001). Conformation, localization, and integrin binding of talin depend on its interaction with phosphoinositides. *The Journal of Biological Chemistry*, 276(24), 21217–21227.

Martin-Bermudo, M. D., Dunin-Borkowski, O. M., & Brown, N. H. (1998). Modulation of integrin activity is vital for morphogenesis. *The Journal of cell biology*, 141(4), 1073-1081.

Mehrbod, M., Trisno, S., & Mofrad, M. R. 2013. On the activation of integrin αIIbβ3: outside-in and inside-out pathways. *Biophysical Journal*, 105(6), 1304–1315.

Michopoulou, A., Montmasson, M., Garnier, C., Lambert, E., Dayan, G., & Rousselle, P. (2020). A novel mechanism in wound healing: Laminin 332 drives MMP9/14 activity by recruiting syndecan-1 and CD44. *Matrix Biology*, 94, 1-17.

Morse, E. M., Brahme, N. N., & Calderwood, D. A. (2014). Integrin cytoplasmic tail interactions. *Biochemistry*, 53(5), 810-820.

Murphy, D. A., & Courtneidge, S. A. (2011). The'ins' and'outs' of podosomes and invadopodia: characteristics, formation and function. *Nature reviews Molecular cell biology*, 12(7), 413-426.

Nagano, M., Hoshino, D., Koshikawa, N., Akizawa, T., & Seiki, M. (2012). Turnover of focal adhesions and cancer cell migration. *International journal of cell biology*, 2012.

Nieberler, M., Reuning, U., Reichart, F., Notni, J., Wester, H. J., Schwaiger, M., Weinmüller, M., Räder, A., Steiger, K., & Kessler, H. (2017). Exploring the Role of RGD-Recognizing Integrins in Cancer. *Cancers*, 9(9), 116.

Parrinello, M., & Rahman, A. (1980). Crystal structure and pair potentials: A molecular-dynamics study. *Physical review letters*, 45(14), 1196.

Parrinello, M., & Rahman, A. (1981). Polymorphic transitions in single crystals: A new molecular dynamics method. *Journal of Applied physics*, 52(12), 7182-7190.

Patil, S., Jedsadayanmata, A., Wencel-Drake, J. D., Wang, W., Knezevic, I., & Lam, S. C. (1999). Identification of a talin-binding site in the integrin beta(3) subunit distinct from the NPLY regulatory motif of post-ligand binding functions. The talin n-terminal head domain interacts with the membrane-proximal region of the beta(3) cytoplasmic tail. *The Journal of Biological Chemistry*, 274(40), 28575–28583.

Pinon, P., Pärssinen, J., Vazquez, P., Bachmann, M., Rahikainen, R., Jacquier, M. C., Azizi, L., Määttä, J. A., Bastmeyer, M., Hytönen, V. P., & Wehrle-Haller, B. (2014). Talin-bound NPLY motif recruits integrin-signaling adapters to regulate cell spreading and mechanosensing. *The Journal of cell biology*, 205(2), 265–281.

Rangarajan, E. S., Primi, M. C., Colgan, L. A., Chinthalapudi, K., Yasuda, R., & Izard, T. (2020). A distinct talin2 structure directs isoform specificity in cell adhesion. *Journal of Biological Chemistry*, 295(37), 12885-12899.

Ren, X. D., Kiosses, W. B., Sieg, D. J., Otey, C. A., Schlaepfer, D. D., & Schwartz, M. A. (2000). Focal adhesion kinase suppresses Rho activity to promote focal adhesion turnover. *Journal of cell science*, 113(20), 3673-3678.

Rens, E. G., & Merks, R. M. (2020). Cell shape and durotaxis explained from cell-extracellular matrix forces and focal adhesion dynamics. *Iscience*, 23(9), 101488.

Ruoslahti, E., & Pierschbacher, M. D. (1987). New perspectives in cell adhesion: RGD and integrins. *Science*, 238(4826), 491-497.

Saltel, F., Mortier, E., Hytönen, V. P., Jacquier, M. C., Zimmermann, P., Vogel, V., Liu, W., & Wehrle-Haller, B. (2009). New PI(4,5)P2- and membrane proximal integrin-binding motifs in the talin head control beta3-integrin clustering. *The Journal of cell biology*, 187(5), 715–731.

Saunders, R. M., Holt, M. R., Jennings, L., Sutton, D. H., Barsukov, I. L., Bobkov, A., Liddington, R. C., Adamson, E. A., Dunn, G. A., & Critchley, D. R. (2006). Role of vinculin in regulating focal adhesion turnover. *European journal of cell biology*, 85(6), 487-500.

Schwartz, M. A. (1997). Integrins, oncogenes, and anchorage independence. *The Journal of cell biology*, 139(3), 575-578.

Stricker, J., Beckham, Y., Davidson, M. W., & Gardel, M. L. (2013). Myosin II-mediated focal adhesion maturation is tension insensitive. *PloS one*, 8(7), e70652.

Sun, Z., Costell, M., & Fässler, R. (2019). Integrin activation by talin, kindlin and mechanical forces. *Nature cell biology*, 21(1), 25-31.

Tadokoro, S., Shattil, S.J., Eto, K., Tai, V., Liddington, R.C., de Pereda, J.M., Ginsberg, M.H. and Calderwood, D.A., (2003). Talin binding to integrin ß tails: a final common step in integrin activation. *Science*, 302(5642), 103-106.

Takada, Y., Ye, X., & Simon, S. (2007). The integrins. *Genome biology*, 8(5), 215.

Tan, Y., Kong, C. W., Chen, S., Cheng, S. H., Li, R. A., & Sun, D. (2012). Probing the mechanobiological properties of human embryonic stem cells in cardiac differentiation by optical tweezers. *Journal of biomechanics*, 45(1), 123-128.

Theodosiou, M., Widmaier, M., Böttcher, R. T., Rognoni, E., Veelders, M., Bharadwaj, M.,

Lambacher, A., Austen, K., Müller, D. J., Zent, R., & Fässler, R. (2016). Kindlin-2 cooperates with talin to activate integrins and induces cell spreading by directly binding paxillin. *eLife*, 5, e10130.

Tidball, J. G. (2005). Mechanical signal transduction in skeletal muscle growth and adaptation. *Journal of Applied Physiology*, 98(5), 1900-1908.

Tselepis, V. H., Green, L. J., & Humphries, M. J. (1997). An RGD to LDV motif conversion within the disintegrin kistrin generates an integrin antagonist that retains potency but exhibits altered receptor specificity: evidence for a functional equivalence of acidic integrin-binding motifs. *Journal of Biological Chemistry*, 272(34), 21341-21348.

van der Flier, A., & Sonnenberg, A. (2001). Function and interactions of integrins. *Cell and Tissue Research*, 305(3), 285–298.

Vincent, C., Siddiqui, T. A., & Schlichter, L. C. (2012). Podosomes in migrating microglia: components and matrix degradation. *Journal of neuroinflammation*, 9(1), 1-15.

Wang, J. H. (2012). Pull and push: talin activation for integrin signaling. *Cell research*, 22(11), 1512-1514.

Wang, J. H. C., & Thampatty, B. P. (2006). An introductory review of cell mechanobiology. *Biomechanics and modeling in mechanobiology*, 5(1), 1-16.

Wang, J., Wolf, R.M., Caldwell, J.W., Kollman, P.A. and Case, D.A., (2004). Development and testing of a general amber force field. *Journal of computational chemistry*, 25(9), pp.1157-1174.

Wegener, K. L., Basran, J., Bagshaw, C. R., Campbell, I. D., Roberts, G. C., Critchley, D. R., & Barsukov, I. L. (2008). Structural basis for the interaction between the cytoplasmic domain of the hyaluronate receptor layilin and the talin F3 subdomain. *Journal of molecular biology*, 382(1), 112-126.

Wegener, K. L., Partridge, A. W., Han, J., Pickford, A. R., Liddington, R. C., Ginsberg, M. H., & Campbell, I. D. (2007). Structural basis of integrin activation by talin. *Cell*, 128(1), 171-182.

Yang, J., Zhu, L., Zhang, H., Hirbawi, J., Fukuda, K., Dwivedi, P., Liu, J., Byzova, T., Plow, E. F., Wu, J., & Qin, J. (2014). Conformational activation of talin by RIAM triggers integrin-mediated cell adhesion. *Nature communications*, 5, 5880.

Yao, M., Goult, B. T., Klapholz, B., Hu, X., Toseland, C. P., Guo, Y., Cong, P., Sheetz, M. P., & Yan, J. (2016). The mechanical response of talin. *Nature communications*, 7, 11966.

Ylänne, J., Huuskonen, J., O'Toole, T. E., Ginsberg, M. H., Virtanen, I., & Gahmberg, C. G. (1995). Mutation of the cytoplasmic domain of the integrin beta 3 subunit. Differential effects on cell spreading, recruitment to adhesion plaques, endocytosis, and phagocytosis. *The Journal of biological chemistry*, 270(16), 9550–9557.

Zaidel-Bar, R., Itzkovitz, S., Ma'ayan, A., Iyengar, R., & Geiger, B. (2007). Functional atlas of the integrin adhesome. *Nature cell biology*, 9(8), 858-867.

Zhang, H., Chang, Y. C., Huang, Q., Brennan, M. L., & Wu, J. (2016). Structural and functional analysis of a talin triple-domain module suggests an alternative talin autoinhibitory configuration. *Structure*, 24(5), 721-729.

Zhang, P., Azizi, L., Kukkurainen, S., Gao, T., Baikoghli, M., Jacquier, M. C., Sun, Y., Määttä, J., Cheng, R. H., Wehrle-Haller, B., Hytönen, V. P., & Wu, J. (2020). Crystal structure of the FERM-folded talin head reveals the determinants for integrin binding. *Proceedings of the National Academy of Sciences of the United States of America*, 117(51), 32402–32412.

APPENDIX 1. STRUCTURAL SNAPSHOTS OF FOUR SMD RUNS

The six time points for these snapshots during the SMD simulations (Figures 14-19) were chosen based on the events in the pulling force profile (Figure 6). The overall effect of the SMD simulations is the total unfolding of integrin membrane proximal helix, partial unfolding of talin C-terminal helix and the unbinding of integrin from talin.

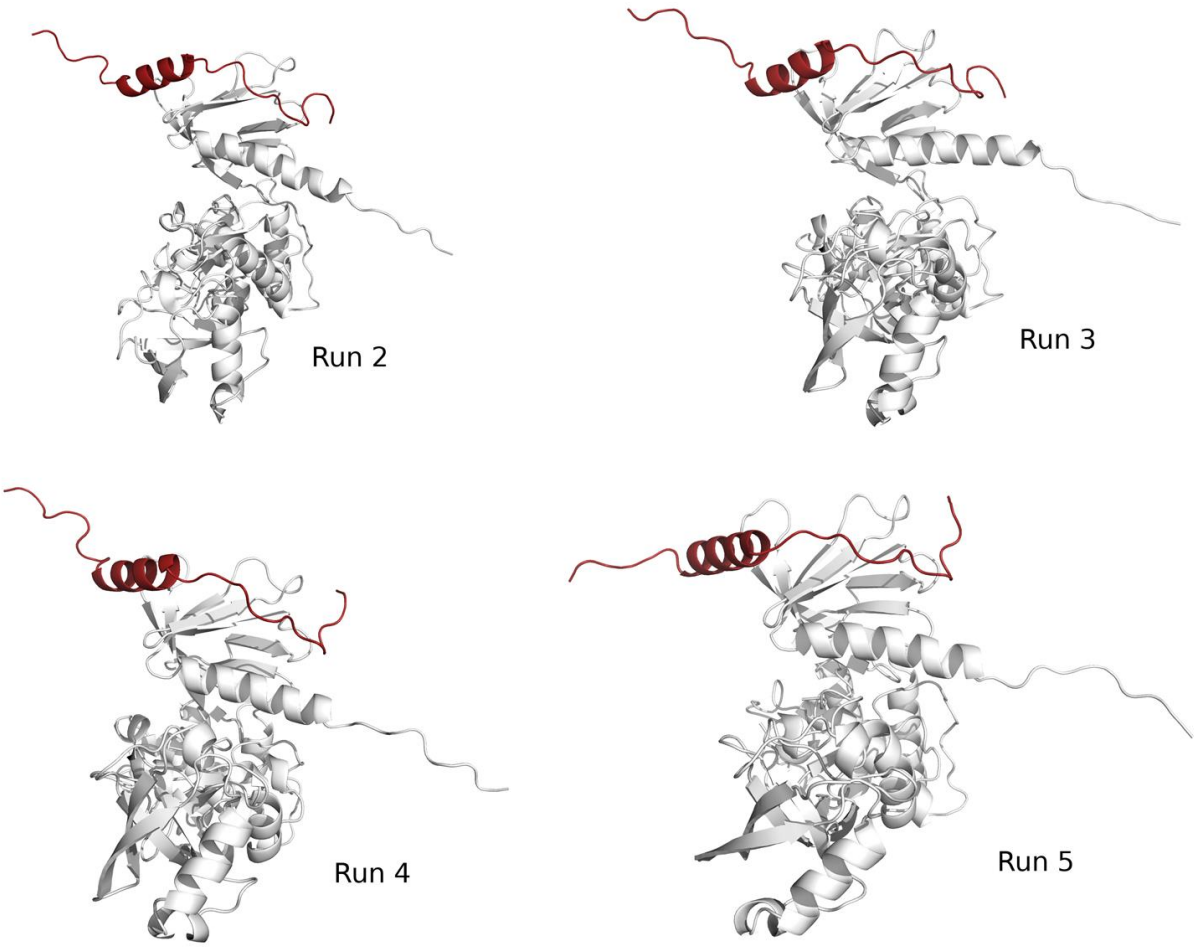

Figure 14. Structural snapshots of four SMD runs before the first peak. Integrin is depicted in red and talin in white. The same coloring applies to Figures 14-19.

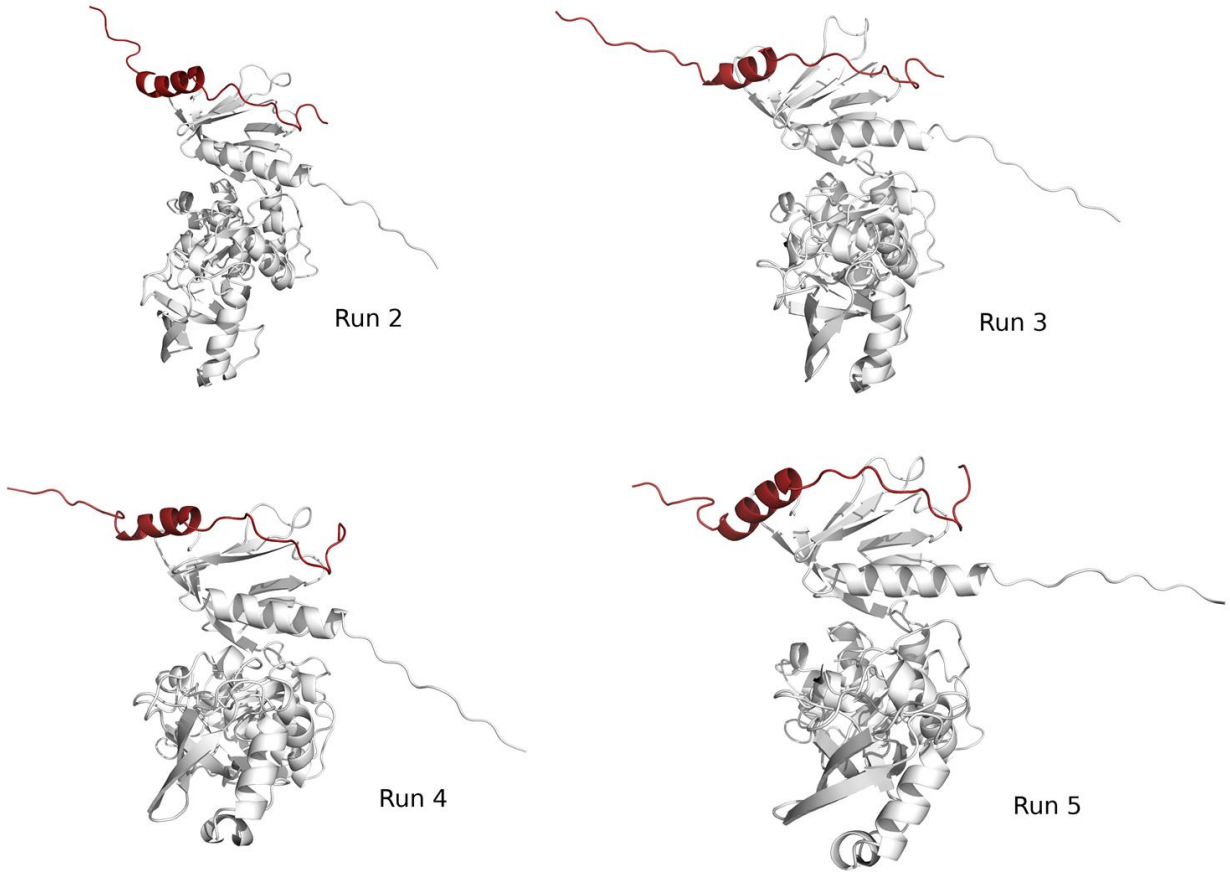

Figure 15. Structural snapshots of four SMD runs at the first peak

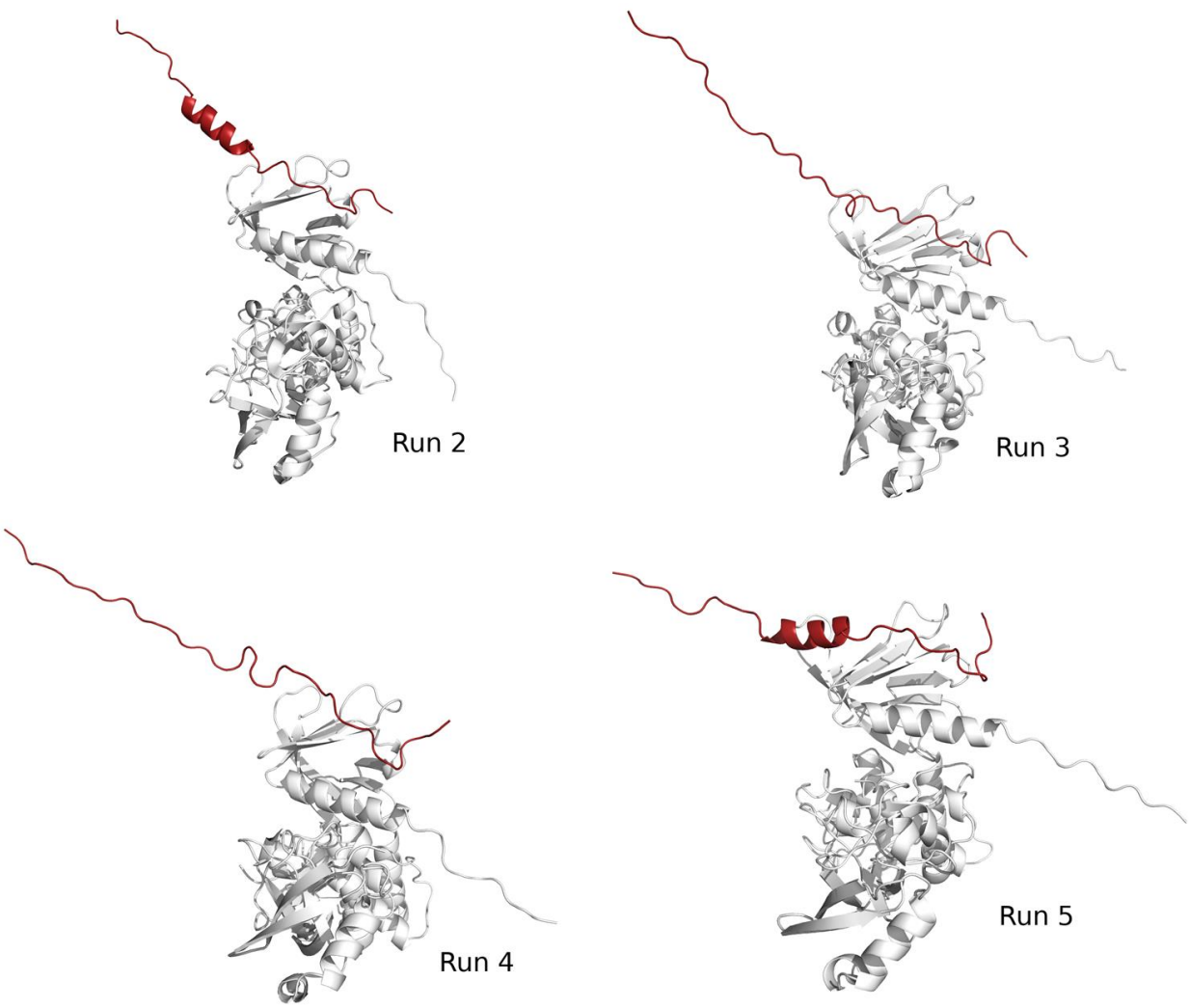

Figure 16. Structural snapshots of four SMD runs after the first peak

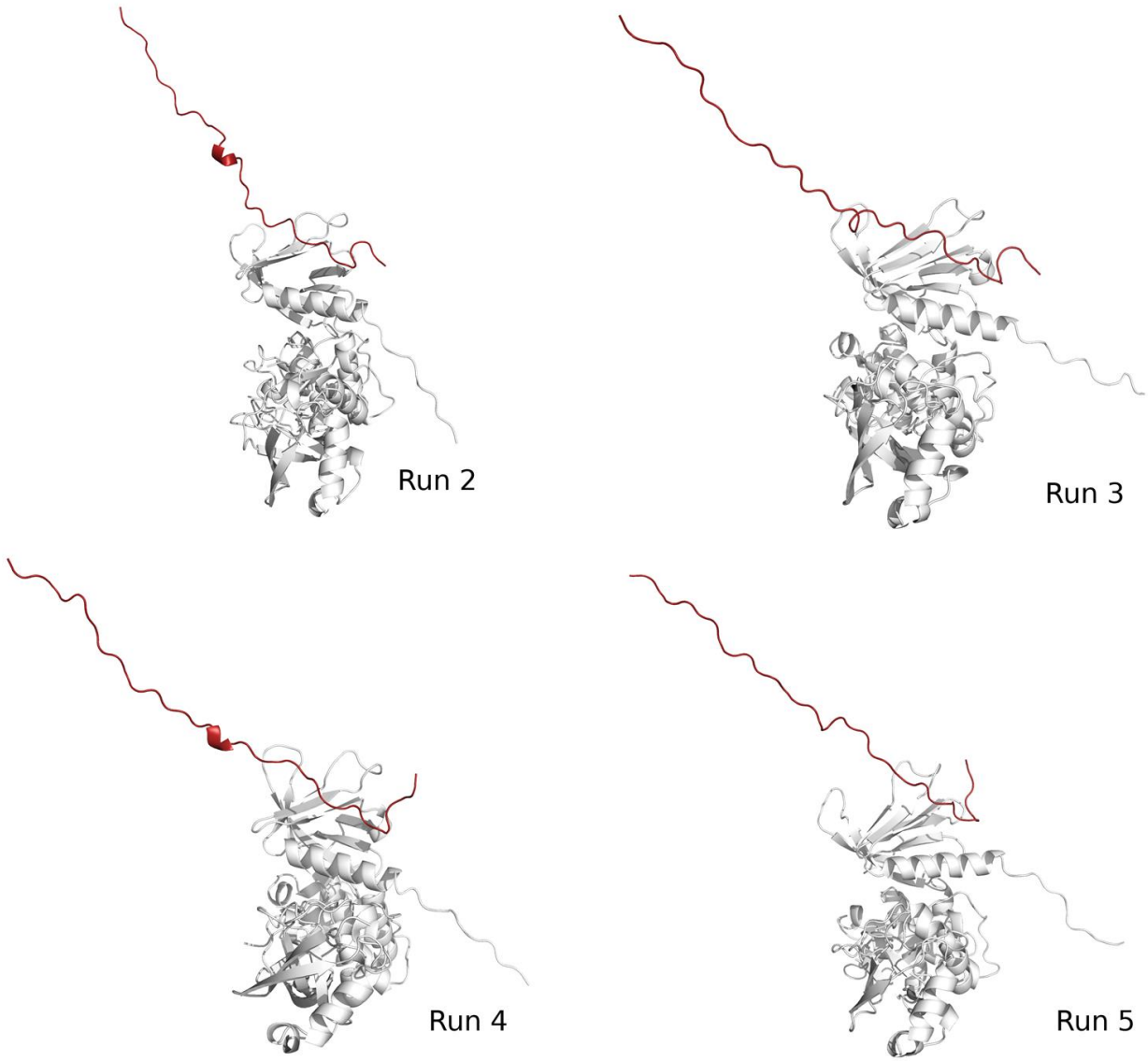

Figure 17. Structural snapshots of four SMD runs before the second peak

Figure 18. Structural snapshots of four SMD runs at the second peak

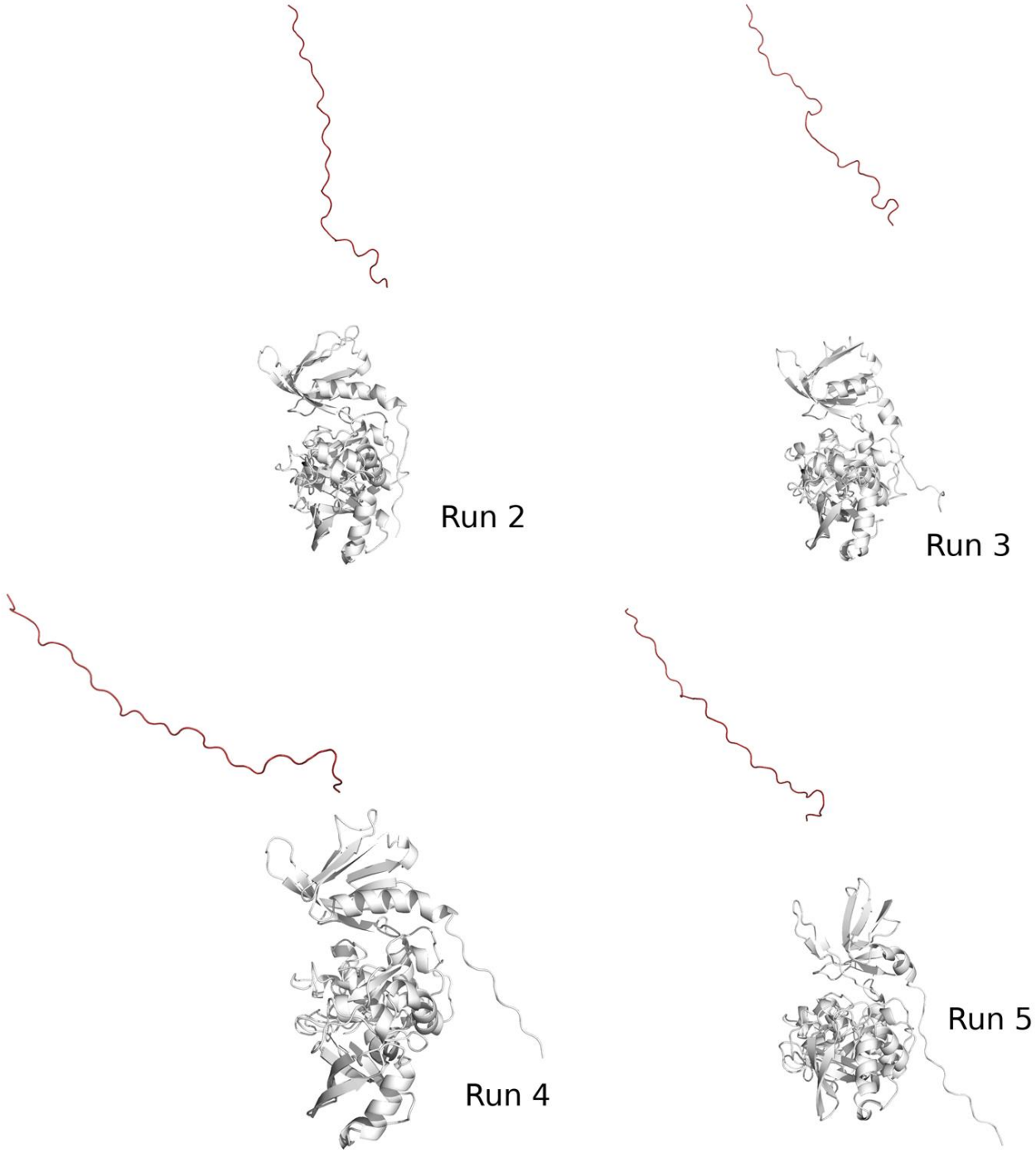

Figure 19. Structural snapshots of four SMD runs after the second peak